

Article

U-Pb Zircon Geochronology of Detrital and Ash Fall Deposits of the Southern Paraná Basin: A Contribution for Provenance, Tectonic Evolution, and the Paleogeography of the SW Gondwana

Ruy Paulo Philipp^{1,*}, Ubiratan Ferrucio Faccini², Cesar Leandro Schultz¹, Gustavo Zvirtes³, Matheus Philippe Bruckmann¹ , Ernesto Lavina², Joice Cagliari², Andrea Ritter Jelinek¹ , Renata Guimarães Netto² , Adriano Roessler Viana⁴  and Miguel Angelo Stipp Basei⁵

- ¹ Centro de Estudos em Petrologia e Geoquímica (CPGq), Instituto de Geociências, Universidade Federal do Rio Grande do Sul (UFRGS), Porto Alegre 90010-150, RS, Brazil; cesar.schultz@ufrgs.br (C.L.S.); matheusbruck@gmail.com (M.P.B.); andrea.jelinek@ufrgs.br (A.R.J.)
- ² Programa de Pós-Graduação em Geologia, Departamento de Geologia, Universidade do Vale do Rio dos Sinos (UNISINOS), São Leopoldo 93022-750, RS, Brazil; ufaccini@unisinis.br (U.F.F.); lavina@unisinis.br (E.L.); joiceca@unisinis.br (J.C.); nettorg@unisinis.br (R.G.N.)
- ³ Department of Geology and Geophysics, University of Aberdeen (UoA), Aberdeen AB24 3FX, UK; gustavo.zvirtes1@abdn.ac.uk
- ⁴ PETROBRAS S.A., Rio de Janeiro 20031-912, RJ, Brazil; vianaadri@hotmail.com
- ⁵ Centro de Pesquisas Geocronológicas (CPGEO), Instituto de Geociências, USP, São Paulo 13083-896, SP, Brazil; baseimas@usp.br
- * Correspondence: ruy.philipp@ufrgs.br



Citation: Philipp, R.P.; Faccini, U.F.; Schultz, C.L.; Zvirtes, G.; Bruckmann, M.P.; Lavina, E.; Cagliari, J.; Jelinek, A.R.; Netto, R.G.; Viana, A.R.; et al. U-Pb Zircon Geochronology of Detrital and Ash Fall Deposits of the Southern Paraná Basin: A Contribution for Provenance, Tectonic Evolution, and the Paleogeography of the SW Gondwana. *Geosciences* **2023**, *13*, 225. <https://doi.org/10.3390/geosciences13080225>

Academic Editors: Jesus Martinez-Frias and Markes E. Johnson

Received: 3 May 2023

Revised: 1 July 2023

Accepted: 3 July 2023

Published: 27 July 2023



Copyright: © 2023 by the authors. Licensee MDPI, Basel, Switzerland. This article is an open access article distributed under the terms and conditions of the Creative Commons Attribution (CC BY) license (<https://creativecommons.org/licenses/by/4.0/>).

Abstract: Zircon U-Pb geochronology was applied to investigate the provenance, depositional ages, and paleogeography of the southwestern Gondwana in detrital and ash fall sediments from Carboniferous to Jurassic succession of the southern Paraná Basin. Four detrital age populations suggest provenance from local and distal sources located to the south, southeast, and southwest: (i) Archean to Paleoproterozoic zircons from the Rio de La Plata Craton, Nico Peres and Taquarembó terranes; (ii) Grenvillian zircons from the basement of the Gondwanides and Namaqua–Natal belts; (iii) Neoproterozoic grains from the Don Feliciano Belt; and (iv) Phanerozoic populations from Paleozoic orogenic belts and related foreland systems in Argentina, as well as eroded units of the Paraná Basin. The paleogeographic reconstruction indicates an evolution in three distinct stages: (1) a gulf open to the Panthalassa Ocean during the Carboniferous; (2) an epicontinental sea with the rise of the Gondwanides Orogeny during the Permian; and (3) continental deposits controlled by an intra-plate graben system during the Triassic. Permian–Triassic volcanogenic zircons provide constrained maximum depositional ages and attested persistent volcanism, related to the Choiyoi magmatism and effects of the climate change episodes. During the Triassic, the extensional graben system recorded the uplift of the basement through regional northwest and northeast fault systems, and the recycling of Permian zircons, modifying source-to-sink relationships.

Keywords: paraná basin; zircon geochronology; gondwana; gondwanides belt; provenance; ash fall layers; maximum depositional ages; paleogeography

1. Introduction

The Paraná Basin (PB) is one of the largest depositional sites during Gondwana sedimentation. The basin developed over an intracratonic area that stabilized after the Brasi-liano–Pan-African Cycle, recording the effects and influences of tectonic activity on sedimentation, basin architecture, and global changes in environmental conditions [1–3]. The PB evolved alongside its correlative basins (e.g., the Karoo Basin in Africa and Mozambique) along a common Paleozoic Gondwana active margin facing the Panthalassa Ocean [4]

(Figure 1). The basin originated as a gulf open to the Panthalassa and underwent progressive closure to marine incursion induced by the marginal convergent tectonics, eventually becoming an intracratonic depression trapped within Gondwana over time [2]. This margin was transformed into a series of fold-and-thrust belts, magmatic arcs, and related collisional basins associated with the development of the Gondwanides Belt [4–6]. The basin evolved under the influence of intraplate stresses, which led to continental flexural deformation and extension due to the onset of the marginal orogenic processes [5,6]. The chronostratigraphic positioning of sediments from the Paraná Basin still presents a series of questions due to the lack of effective biostratigraphic elements linked to international geological time scales [1]. The sedimentary succession of the PB provides a precious record that can be investigated to constrain depositional ages and reveal evidence of sedimentary provenance and tectonic processes as proxies for the paleogeographic reconstruction of southwestern Gondwana.

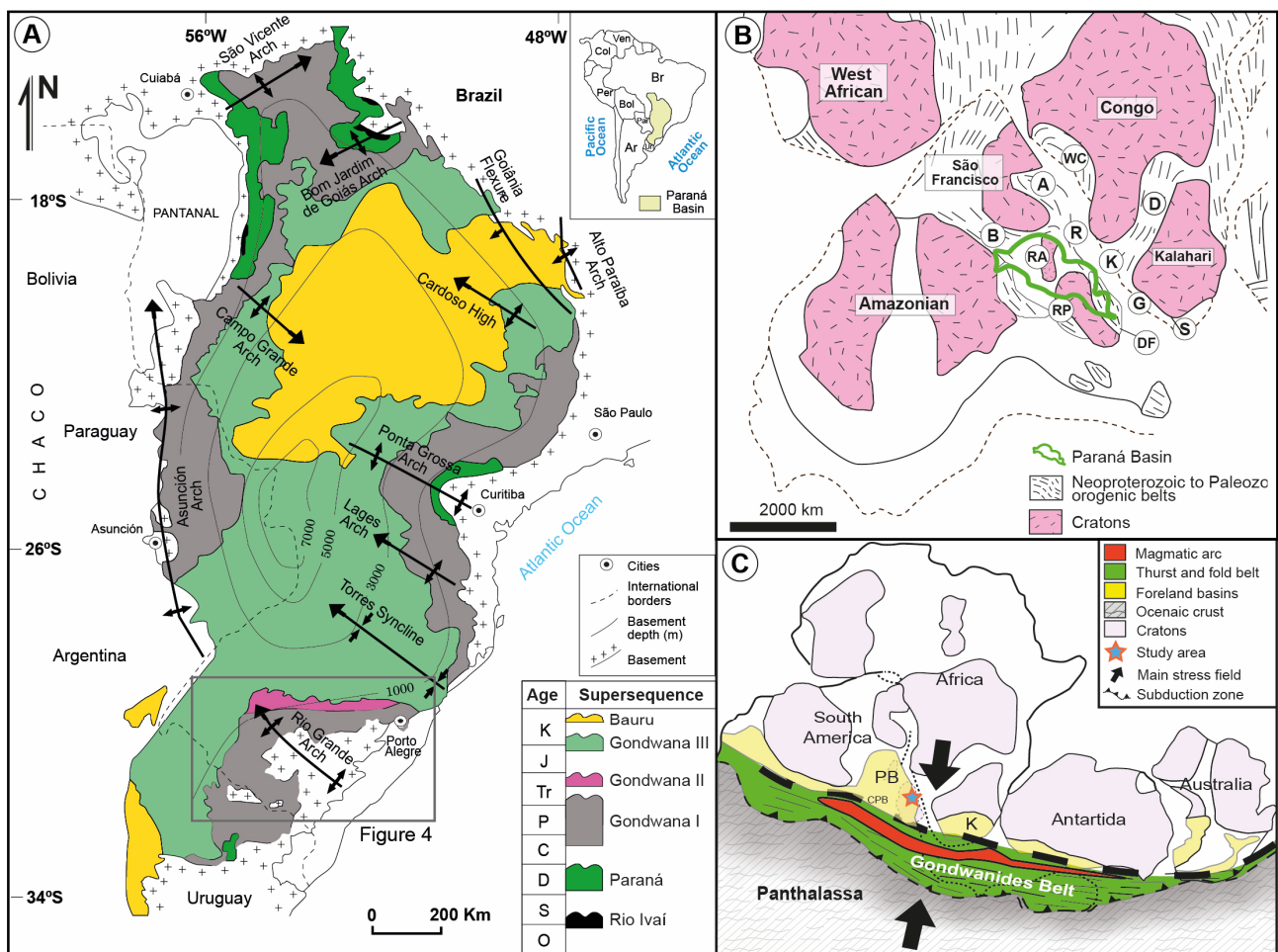


Figure 1. (A) Simplified map of the Paraná Basin showing the six Supersequences proposed by [1] and the structural framework defined by regional structural highs. The study area in the south of the basin is marked by gray rectangle. (B) Precambrian tectonic framework of the SW Gondwana continent showing the cratons and associated orogenic belts, as well as the relative position and actual limits of the Parana Basin (green outline). Brasiliano–Pan-African belts: A = Araçuaí, B = Brasília, DF = Dom Feliciano, G = Gariép, K = Kaoko, R = Ribeira, S = Saldania, and WC = West Congo. RA = Rio Apa Craton (modified from [7]). (C) Schematic tectonic setting of the SW Gondwana margin during the Gondwanic Cycle (Carboniferous to Triassic), marking the position of the collisional basins system (yellow) developed onto the hinterland of the supercontinent, isolated from the Panthalassa Ocean by the Gondwanides Belt. Highlighted basins: PB = Parana Basin; K = Karoo Basin; CB = Chaco Basin. Modified from [4].

This research presents new zircon U-Pb geochronology data obtained via LA-ICP-MS analysis of detrital grains and ash fall crystals from the complete lithostratigraphic succession, including the Carboniferous to Cretaceous units of the southern sector of the Paraná Basin in southern Brazil. The aim is to contribute to the understanding of the evolution of the Paraná Basin as a dynamic system within the context of the southwestern Gondwana margin. Detrital zircon is a common component of clastic sedimentary rocks and plays a significant role in studies of sedimentary provenance and crustal evolution [8–11]. Due to its resistance to erosion, weathering, and alteration processes, zircon grains are useful in tracing the transport routes of clastic material from its source to the final depositional environment [12]. Compilation of crystallization ages for detrital and igneous zircons reveals similar patterns of peaks and gaps, indicating that the sedimentary record is a reliable representation of the magmatic record of the main orogenic cycles [9,10,13,14]. Isotopic investigations of terrigenous and volcanogenic deposits in the Paraná Basin are crucial for improving the determination of provenance indicators and refining depositional ages, thereby enabling paleogeographic and tectonic reconstructions [8–13]. Volcanogenic zircons, preserved in ash fall layers from Permian to Triassic units in the basin provide essential information for refining maximum depositional ages and establishing relationships with volcanic events and paleoenvironmental changes.

This study represents the first comprehensive U-Pb geochronology analysis of the entire sedimentary succession in the southernmost sector of the Paraná Basin in south Brazil. The obtained data reveal isotopic signatures corresponding to the Gondwana I, Gondwana II, and Gondwana III Supersequences deposited during the Late Carboniferous to Lower Cretaceous [1,2,4,5]. The new U-Pb results, comprising approximately 1047 (837 concordant) detrital and volcanogenic zircon grains, were integrated with stratigraphic, sedimentological, and thermochronological data. Given the abundance of available petrological, stratigraphic, structural, paleontological, and geochronological data [15–17], the PB represents a crucial target for applying zircon U-Pb geochronology to refine provenance indicators, constrain depositional ages, evaluate tectono-stratigraphic domains, and assess ancient source-to-sink systems, mainly of the Triassic succession.

2. Geological Context

The Paraná Basin (PB) is a large depositional site located in the southwestern portion of the Gondwana supercontinent. It represents a long period of approximately 350 Ma of sedimentary accumulation and exhibits evidence of marginal tectonic processes, significant climatic changes, and biostratigraphic variations from the Upper Ordovician to the Upper Cretaceous (Figure 1). The basin extends approximately 1750 km in length and 900 km in width, following a N20° E-trending axis, and covers an area of approximately 1.4 million km² [1]. The stratigraphic succession reaches a thickness of around 8 km and consists of a sedimentary sequence covered by basic and acidic volcanic rocks.

The PB is a typical intracratonic basin that has been strongly influenced by marginal orogenic events, particularly the Famatinian Orogeny (Ordovician-Devonian) during the deposition of the Rio Ivaí and Paraná Supersequences, and the Gondwanides Orogeny (Carboniferous-Triassic) during the deposition of the Gondwana I and II Supersequences (Figure 2). In the studied area of the southern sector of the PB, the sedimentary succession primarily reflects the effects of the Gondwanides Orogeny, with the earliest sedimentary units of the Itararé Group deposited during the Upper Carboniferous. The paleogeography of the basin initially involved a gulf open to the south, towards the Panthalassa Ocean. However, as the Gondwanides Orogeny developed along the southwestern margin of the Gondwana shield, the gulf closed during the Permian, isolating the basin from the Panthalassa Ocean by the rise of the Gondwanides Belt [2]. During the Triassic, a transition to extensional tectonics occurred, resulting in the formation of a series of synclises and arcs through basement uplift and extensional graben systems controlled by the late extensional collapse phase (Figure 2).

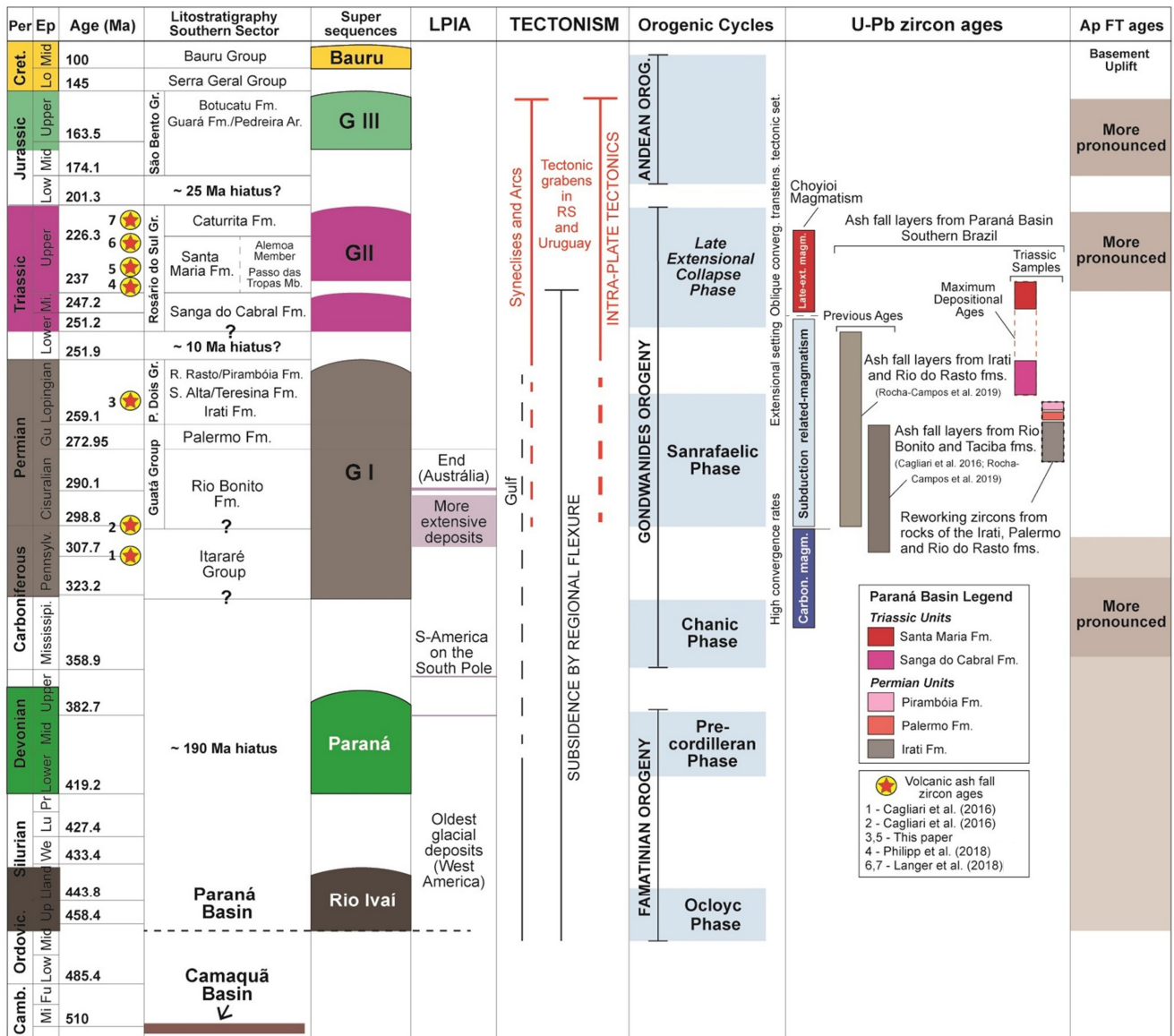


Figure 2. Comparative chart depicting the lithostratigraphic framework, tectonic setting, orogenic and magmatic events, ash fall U-Pb zircon ages, and apatite fission track data associated with the Paleozoic-Mesozoic units of the Paraná Basin (data compiled from [18–28]).

From the entire succession of the basin, six Supersequences have been defined by [1]: Rio Ivaí (Ordovician–Silurian), Paraná (Devonian), Gondwana I (Upper Carboniferous–Lower Triassic), Gondwana II (Upper Triassic), Gondwana III (Jurassic–Lower Cretaceous), and Baurú (Upper Cretaceous) (Figures 1 and 2). The first three are characterized by marine transgressive–regressive sequences, while the last three consist of continental siliciclastic sedimentation and associated igneous rocks [5,6]. The definition of each time interval has been primarily based on low-resolution dataset, such as palynomorphs, plants, invertebrate, and vertebrate macrofossils [16,29–32]. It is important to note that in the southern sector of the PB, the first two Supersequences are not recorded (Figures 1B and 2).

In the study area, sedimentary and volcanic rocks from the Paraná Basin occur deposited over the basement units of the Dom Feliciano Belt and of the Rio de La Plata Craton (Figure 3) representing over 200 million years of the Earth’s history (Figure 4). This interval includes two significant climatic changes: (i) the Late Paleozoic Ice Age (LPIA) in Western Gondwana [33] and (ii) the global warming that occurred from the end of the Permian to the Upper Jurassic. The basal portion of the basin comprises the Taciba

Formation, part of the Itararé Group, which was deposited in a glacial environment at the end of the Carboniferous related to a LPIA [17,33,34] (Figure 5). The glacial succession was overlain by coastal and shallow marine facies, with significant Permian deposits of coal and fluvial sediments from the Guatá Group (Rio Bonito and Palermo formations), showing predominant sediment transport towards the north and northwest [30–32,35]. The end of the Gondwana I Supersequence is marked by the Permian units of the Passa Dois Group, representing the last marine incursion from the south by the Panthalassa Ocean. This is characterized by shallow marine and coastal deposits of the Irati, Serra Alta and Teresina formations, followed by an oceanic retreat associated with the peak of the Gondwanides Orogeny. This retreat is represented by continental lacustrine, fluvial, and aeolian facies of the Rio do Rasto and Pirambóia formations, indicating the establishment of more arid conditions [19,36,37].

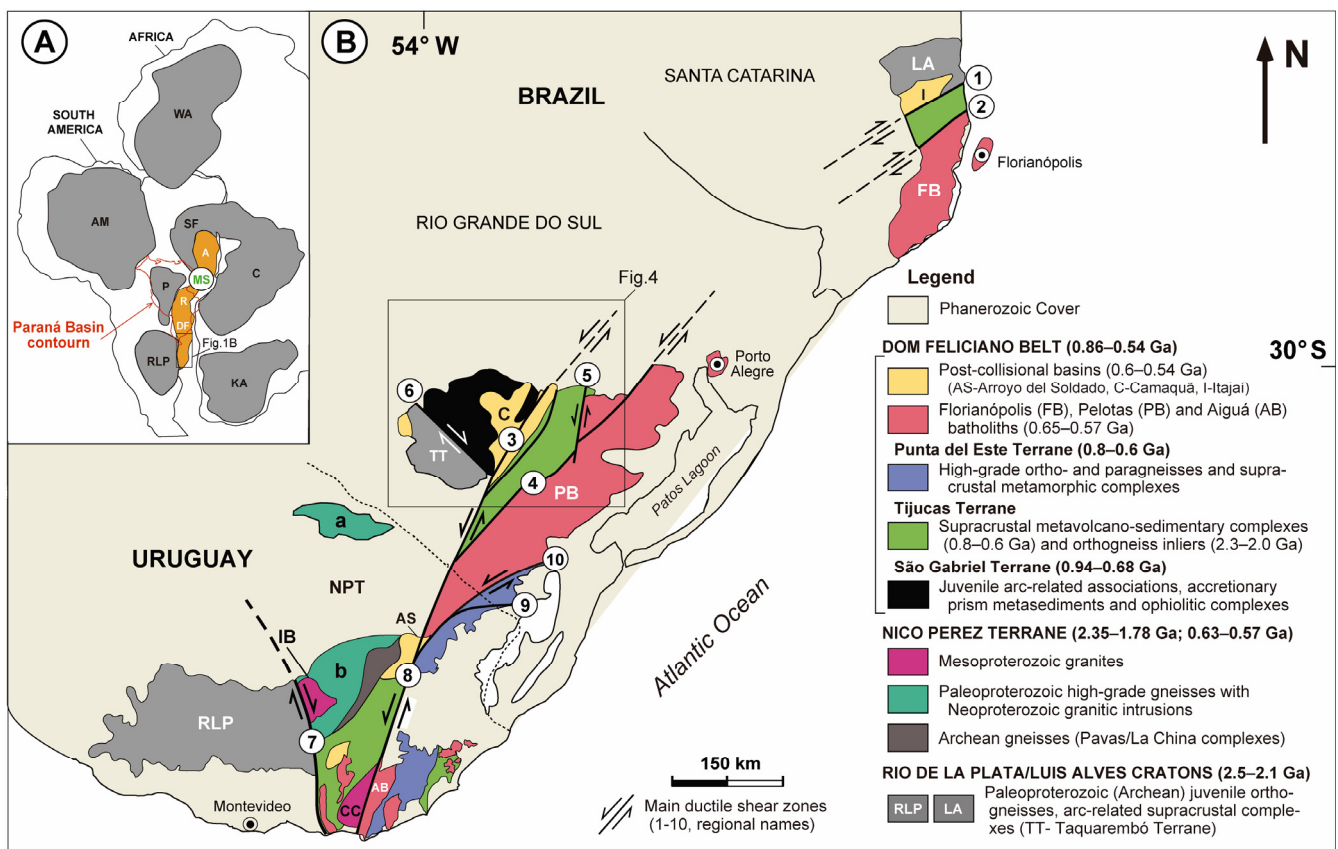


Figure 3. (A) Location of the Mantiqueira Orogenic System (MS) and of the surrounding cratons. The red line indicates the current extent of the exposures of the Parana Basin. Cratons: AM: Amazon, C: Congo, KA: Kalahari, LA: Luis Alves, P: Paranapanema, RLP: Rio de la Plata, SF: São Francisco, WA: West African. MS: Mantiqueira Orogenic System. Belts: A: Araçuaí, DF: Dom Feliciano, R: Ribeira. (B) geological map of the southern Brazilian and Uruguayan shields; map and data compiled from [38,39]. Ductile Shear Zones: 1—Itajai-Perimbó, 2—Major Gercino, 3—Caçapava do Sul, 4—Dorsal de Canguçu, 5—Passo do Marinheiro, 6—Ibaré, 7—Sarandí del Yí, 8—Sierra Ballena, 9—Cerro Amaro, 10—Arroio Grande.

The isolation of the basin in an epicontinental sea was accompanied by significant climate change related to the increase in volcanic activity during the Triassic, leading to the transition to desert conditions in the Late Jurassic. The Triassic-Jurassic transition is marked by an unconformity associated with the uplift and erosion of the underlying Permian strata, followed by the deposition of the Sanga do Cabral Formation (Lower Triassic). This formation represents an alluvial plain characterized by a sandy river system with braided channels (Figure 5). The succession continues with the Santa Maria Formation (Middle to

Upper Triassic), which consists of a braided fluvial system with low to moderate sinuosity in its lower section and by wide lacustrine facies in its upper section [16]. The red beds at the top portion indicate the transition to an arid climate, leading to the extinction of a diverse fauna of tetrapod reptiles and regional flora [16,29,30]. The fossil content of the area has been of great scientific interest since the early 20th century due to its abundant and unique Middle–Late Triassic vertebrate fossils, which do not correlate with facies or chronostratigraphic units in the other regions of the basin [29,30]. This biostratigraphic significance is important for correlation purposes within the broader evolutionary context of the southern Gondwana during the Late Paleozoic and Early Mesozoic eras [16] (Figure 5).

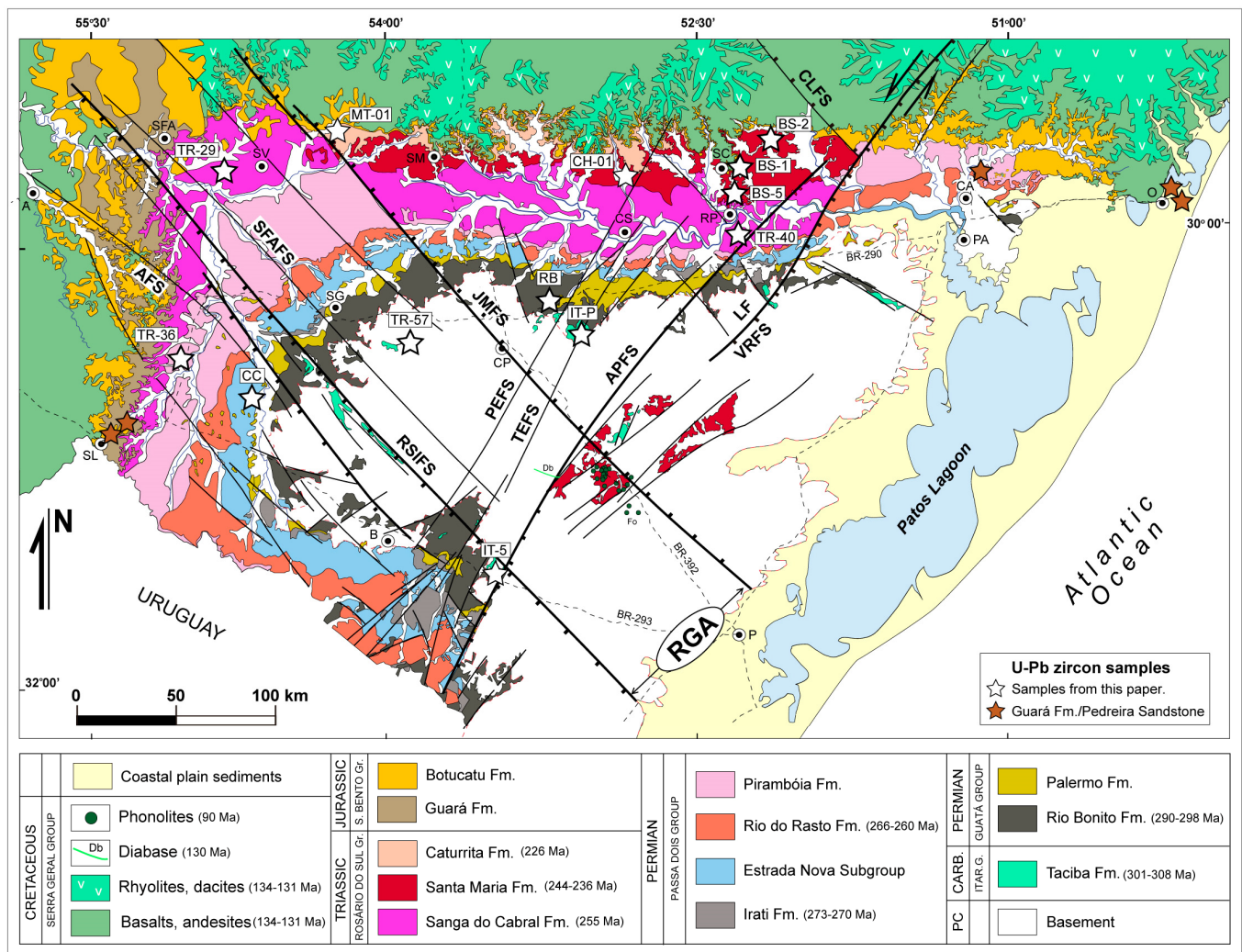


Figure 4. Geological map of the southern sector of the Paraná Basin, highlighting the main tectonic structures that affect the basin and the position of the Rio Grande Arc (RGA). The location of the samples marked with a star symbol. Fault Systems: APFS—Açotéia-Piquiri, AFS—Alegrete, CLFS—Caxias-Lajeado, JMFS—Jaguari-Mata, PEFS—Passo dos Enforcados, RSI—Rosário do Sul-Ibaré, TEFS—Tapera-Emiliano, VRFS—Vigia-Roque, Fault: LF—Leão Fault. Cities: A—Alegrete, B—Bagé, CA—Canoas, CP—Caçapava do Sul, CS—Cachoeira do Sul, P—Pelotas, PA—Porto Alegre, RP—Rio Pardo, SG—São Gabriel, SFA—São Francisco de Assis, SL—Santana do Livramento, SM—Santa Maria, SV—São Vicente. Geological map modified from [40].

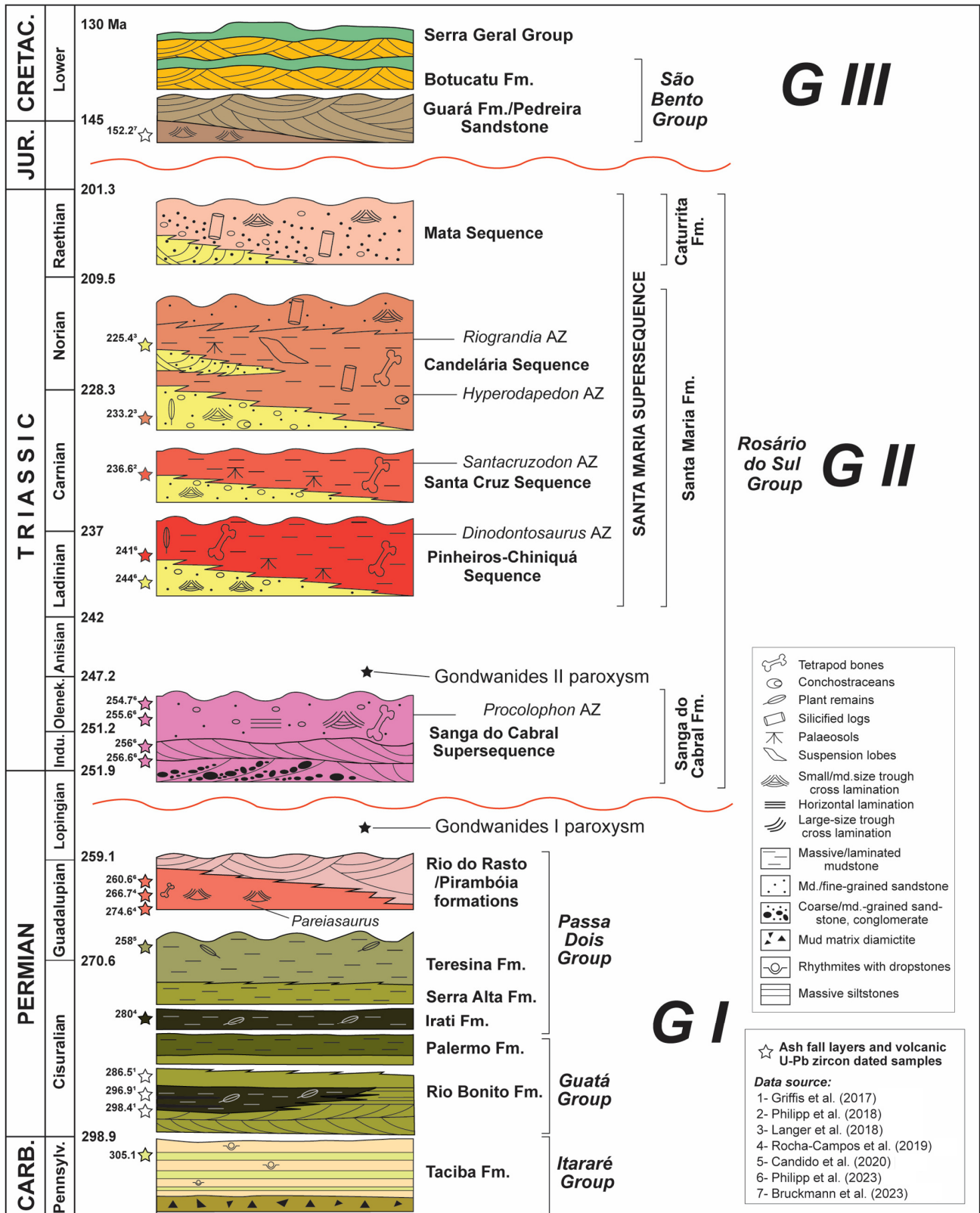


Figure 5. Chronostratigraphic, lithostratigraphic, and sequence stratigraphy units of the southern sector of the Paraná Basin. Ages are from Gradstein et al. (1995), and palaeovertebrate data are from Horn et al. (2014) and Schultz et al. (2000, 2020). The stratigraphy was established using biostratigraphic and geochronologic data.

The Triassic–Jurassic interval was characterized by tectonic activities associated with the late extensional collapse phase of the Gondwanides Orogeny [41], which influenced the deposition of the Sanga do Cabral, Santa Maria, and Caturrita formations from the Rosário do Sul Group [19,36,37]. Intracontinental rifting, manifested by the development of NW–SE oriented extensional faults, controlled the sedimentary transportation routes, resulting in the cyclic deposition of high-energy alluvial and fluvial sequences sourced from the south and southeast [36,37,41]. This sedimentary succession is preserved only in the southern sector of the basin, where an intra-plate extensional graben exerted significant depositional control, as indicated by facies associations and the consistent directions of sediment transport towards the north–northwest [15,16,36,37].

Following an initial phase of crustal uplift that marked the early stages manifestations of the South Atlantic rifting, the São Bento Group (Jurassic) formed, comprising a combination of fluvial and aeolian sediments. This group indicates the transition from semi-arid to arid conditions through the deposition of ephemeral fluvial deposits associated with aeolian systems of the Guara Formation, which eventually evolved into the extensive aeolian dune desert of the Botucatu Formation [42,43]. The deposition of the Botucatu Formation coincides with the emplacement of basic lavas from the Serra Geral Group that erupted during the Lower Cretaceous, marking the onset of the opening of the South Atlantic Ocean [44,45].

3. Materials and Methods

A total of 1047 new detrital U-Pb zircons were analyzed using LA-MC-ICPMS. To construct a comprehensive stratigraphic profile of the basin, published data from [46] and unpublished data for the Rosario do Sul Group [47], as well as data for the Guara Formation and Pedreira Sandstone [48], were compiled, resulting in an expanded database of 1648 concordant analyses. This database was compared with 3235 published zircon data compiled from [17] ($n = 1798$) and [49] ($n = 426$) from the Santa Catarina State sector, as well as the analyses of the southern sector of the PB from the Itarare Group [34] ($n = 1011$).

The zircon grains were obtained by crushing and milling the samples using a jaw crusher, followed by pulverization. Heavy mineral concentrates were obtained from approximately 10 kg of rock samples using conventional crushing (particle size smaller than 500 μm) and panning methods. Zircons were extracted from the 100–200 mesh fractions using standard isodynamic, gravimetric, and magnetic techniques. No morphology or color differentiation was conducted during handpicking to avoid bias. The zircon grains were then mounted on epoxy resin, and their surfaces were then polished to expose the grain interiors. The U-Pb analyses were conducted at the Geochronological Research Center (CP-GEO) at the University of Sao Paulo (USP). Cathodoluminescence (CL) images of the zircon grains, obtained using a Quanta 250 FEG scanning electron microscope equipped with a Mono CL cathodoluminescence spectroscope (Centaurus detector), were used to determine their internal structures. The images were used to identify spots for U/Pb analysis, avoiding fractures, inclusions or metamict areas that may have experienced Pb loss.

Isotopic data were obtained using a Thermo Finnigan Neptune inductively coupled plasma mass spectrometer (ICP-MS) coupled to a Photon-Machines 193 nm laser system. Calibration was performed using the GJ-1 zircon standard [50]. The cup configuration optimized for U-Pb data acquisition was IC3 ^{202}Hg , IC4 $^{204}(\text{Hg} + \text{Pb})$, L4 ^{206}Pb , IC6 ^{207}Pb , L3 ^{208}Pb , H2 ^{232}Th , and H4 ^{238}U , where L and H represent low and high mass positions, respectively, and ICs represent ion counting (continuous dynode system). The ICP configuration includes a radio frequency power of 1100 W, a cool gas flow rate of 15 L/min (Ar), an auxiliary gas flow rate of 0.7 L/min (Ar), and a sample gas flow rate of 0.6 L/min. The laser setup parameters were as follows: energy, 6 mJ; repetition rate, 5 Hz; spot size ranging from 25 to 38 μm ; and helium carrier gas flow rate ranging from 0.35 to 0.5 L/min. The routine U-Pb analysis consisted of 2 blanks, 2 NIST (610), 3 secondary/quality control reference materials (GJ-1 zircon) [51], 13 unknown samples, 2 secondary/quality control reference materials and 2 blank measurements. Each run comprised 40 cycles, with 1 s per

cycle. The ^{204}Hg interference on ^{204}Pb was corrected by measuring the ^{202}Hg and using a $^{204}\text{Hg}/^{202}\text{Hg}$ value of 4.2. $^{207}\text{Pb}/^{206}\text{Pb}$ ratio normalization was achieved using combined NIST (612) and external or secondary reference materials were used for quality control. For calibration/normalization, primary reference materials were utilized. The GJ-1 zircon reference material (602 ± 4.4 Ma) was used for mass bias correction associated with uncertainty introduced by the laser-induced fractionation of elements and mass instrumental discrimination. Zircon typically contains low concentrations of common Pb; thus, the reliability of the measured $^{207}\text{Pb}/^{206}\text{Pb}$ and $^{206}\text{Pb}/^{238}\text{U}$ ratios is critically dependent on the accurate assessment of the common Pb component. The residual common Pb was corrected according to the measured ^{204}Pb concentration using the known terrestrial composition [52]. Data with a high content of common Pb were discarded for the histograms. The isotope ratios and inter-element fractionation of data obtained via ICP-MS were evaluated by interspersing the GJ-1 zircon in every set of thirteen zircon samples (spots). The GJ-1 reference material and a second Temora reference material met the requirements for the methods used in our laboratory, and the ratios of $^{206}\text{Pb}^*/^{238}\text{U}$, $^{207}\text{Pb}/^{206}\text{Pb}$ and $^{232}\text{Th}/^{238}\text{U}$ were homogeneous throughout the application of bracket technique. External errors were calculated using the error propagation of the individual measurements of the GJ-1 and NIST 610 reference materials and measurements into the individual zircon samples (spots). Decay constants used for age calculation are those recommended by [53]. Measured ^{204}Pb was applied for the common lead correction, and data reduction was conducted using the Squid and Isoplot programs [54].

The U-Pb ages were plotted on the Concordia diagrams, weighted average and probability density plots. All samples presented yielded reliable ages with less than 5% discordance for $^{206}\text{Pb}/^{238}\text{U}$ to $^{207}\text{Pb}/^{235}\text{U}$ ratios and 10% discordance for $^{206}\text{Pb}/^{238}\text{U}$ to $^{207}\text{Pb}/^{206}\text{Pb}$ ratios. Plots and age calculations were conducted using Isoplot-R based on $^{206}\text{Pb}/^{238}\text{U}$ (<1.3 Ga) and $^{206}\text{Pb}/^{207}\text{Pb}$ (>1.3 Ga) [49,51,55]. Uncertainties for isotopic ratios are presented at the 2 s level (LA-MC-ICPMS) or 1 s level (SHRIMP) with the final age quoted at 95% confidence. The complete data set is included in the Supplementary Data (Tables S1–S15). The new 837 concordant zircons presented were used to construct relative probability diagrams (PDP and KDE), which are represented in Tables S1–S15 (Supplementary Data), as well as Concordia and weighted average diagrams.

4. Results

A total of fifteen (15) samples from eight (8) lithostratigraphic units of the Paraná Basin in Rio Grande do Sul State were analyzed, covering the Upper Carboniferous to Early Cretaceous interval (Figure 4). The analysis of 1047 zircon grains resulted in 837 concordant results (700 from detrital grains and 137 from volcanogenic euhedral crystals) and 210 discordant results. Figure 12 shows the cathodoluminescence images of the representative volcanic zircon crystals analyzed.

4.1. Guatá Group

Rio Bonito Formation

A total of 233 zircons yielded 175 concordant analyses from one sample of fine-grained sandstone (sample RB-P) and five associated samples of ash fall layers (Tnst-1, Tnst-1.5, Tnst-2, Tnst-3, and Tnst-6) from the Capané paleovalley (Figure 4). These samples represent post-glacial deposits over the glaciogenic strata of the Taciba Formation. The analyzed samples provide a representative sequence from the bottom to the top of the succession, covering over 100 m of thickness. The ash fall layers (also known as tonstein) in samples Tnst-1, Tnst-1.5, Tnst-2, Tnst-3, and Tnst-6 were collected from the Barrocada outcrop, which has a 300 m width and a 40 m high cliff exposing the middle and upper sections of the Rio Bonito Formation. These sections contain coal seams associated with fine-grained sandstone overlain by arkosic and quartzose sandstone layers.

Sample Tnst-1 was collected approximately 100 m away from the Barrocada cliff, and sample Tnst-2 was collected at the base of the cliff, stratigraphically 5 m above Tnst-1 [56].

Both tonstein levels occur as thin (2–4 cm) and discontinuous layers of whitish claystone interbedded with siltstones (Tnst-1) or coal seams (Tnst-2). Over 300 crystals with a size range of 70–500 μm were collected, and two groups of zircons were identified. The main population consisted of prismatic, euhedral, and elongated crystals with length-to-width (L:W) ratios ranging from 2:1 to 14:1 (average 5:1), exhibiting pinacoid terminations and magmatic oscillatory zoning. The subordinate group comprises sub-euhedral crystals with pyramidal terminations and sub-rounded grains, both displaying well-defined oscillatory zoning and L:W ratios ranging from 1:1 to 4.8:1 (average 2.4:1). The main group is subordinate in Tnst1 and dominant in Tnst-2. Analysis of 52 zircons from the sample Tsnt-1 yielded 46 concordant results which are displayed in KDE and PDP plots in Figures 6A and 7D1, as well as in Table S4. The Th/U ratios, ranging between 0.22 and 1.27, indicate magmatic crystals. The main Paleozoic population exhibits $^{238}\text{U}/^{206}\text{Pb}$ ages between 289 and 385 Ma. The youngest concordant population a Concordia age (Wheterill) of 301.2 ± 1 Ma (MSDW = 0.0042, $n = 16$). The $^{238}\text{U}/^{206}\text{Pb}$ weighted average age obtained from the five youngest grains is 291 ± 3 Ma (MSWD = 0.46, $n = 5$). Older detrital grain populations show a $^{238}\text{U}/^{206}\text{Pb}$ weighted average age of 362 ± 17 Ma having three Neoproterozoic zircons with ages of 630, 801, and 1025 Ma.

From Tnst-2, a total of 39 zircons were analyzed, resulting in 31 concordant results (Figures 6A and 7D1, in Table S5). The Th/U ratios range between 0.44 and 1.04, typical of magmatic crystals. The analyzed zircons are volcanic in origin, with results showing a dominant Lower Permian $^{238}\text{U}/^{206}\text{Pb}$ age ranging from 280 to 299 Ma, resulting in a Concordia age of 289.5 ± 1.1 Ma (MSWD = 0.99, $n = 24$). The youngest population yielded a Concordia age of 289.9 ± 1.1 Ma (MSDW = 0.86, $n = 21$), while the youngest five grains yielded a Concordia age of 283.4 ± 1.7 Ma (MSWD = 0.15) and a $^{238}\text{U}/^{206}\text{Pb}$ weighted average of 283.4 ± 1.7 Ma (MSWD = 0.20).

The sample Tnst-1.5, collected between samples Tnst-1 and Tnst-2, presents two grain populations with different morphological characteristics. All twenty-five (25) zircons were concordant (Figure 6A, Table S5) from which 7 were used to calculate the youngest population. The other eighteen (18) zircons represent two Neoproterozoic populations. The youngest zircons are euhedral crystals with prismatic and elongated shapes and sector zoning, with sizes varying between 120 and 300 μm and L:W ratios ranging from 2:1 to 14:1 (average 5:1). The oldest zircons comprise sub-rounded grains with sub-euhedral form and pyramidal terminations, both displaying well-defined oscillatory zoning. The sizes vary between 40–100 μm and the L:W range from 1:1 to 5:1. The Th/U ratios vary between 0.40 and 1.08, which are considered typical for igneous crystals. The youngest population shows $^{238}\text{U}/^{206}\text{Pb}$ ages ranging from 287 to 303 Ma and yielded a Concordia age of 296.8 ± 2.2 Ma (MSWD = 1.4, $n = 7$), which is similar to the $^{238}\text{U}/^{206}\text{Pb}$ weighted average age of 296.8 ± 4.4 Ma (MSWD = 0.90, $n = 5$). However, the three youngest grains have a slight discordance. Two concordant zircons provided an age of 301.7 ± 3.5 Ma (MSWD = 0.0038). The results revealed one main population ranging from 574 to 534 Ma and Concordia age of 542.1 ± 3.1 Ma, (MSWD = 0.60, $n = 6$). A second group showed ages of 662 and 628 Ma, resulting in a Concordia age of 636.4 ± 13 Ma (MSWD = 0.0013, $n = 6$). Subordinate ages are Tonian (810 Ma) and Mesoproterozoic (1.277 Ma).

Sample Tnst-3 was collected in ash fall layers between the samples Tnst-1.5 and Tnst-6. Twelve zircons yielded two main detrital populations (Figures 6A and 7D1, and Table S6). The youngest population comprises euhedral crystals with elongated and prismatic shapes, bipyramidal terminations, and well-defined oscillatory zoning. The grain size varies between 120 and 350 μm with L:W ratios ranging from 2:1 to 5:1. The subordinate older population comprises sub-euhedral crystals with pyramidal terminations and sub-rounded grains with well-defined oscillatory zonation. Grain sizes vary between 40 and 100 μm , with L:W ranging between 1:1 and 2:1. The Th/U ratios range between 0.26 and 1.79, indicating igneous crystals. One main population with $^{238}\text{U}/^{206}\text{Pb}$ ages between 574 and 534 Ma showed a Concordia age of 556.6 ± 4 Ma (MSWD = 0.17, $n = 6$). Other detrital zircons show isolated Tonian ages of 638, 720, and 780 Ma, and Mesoproterozoic ages of 1.024, 1.063, and 1.890 Ma.

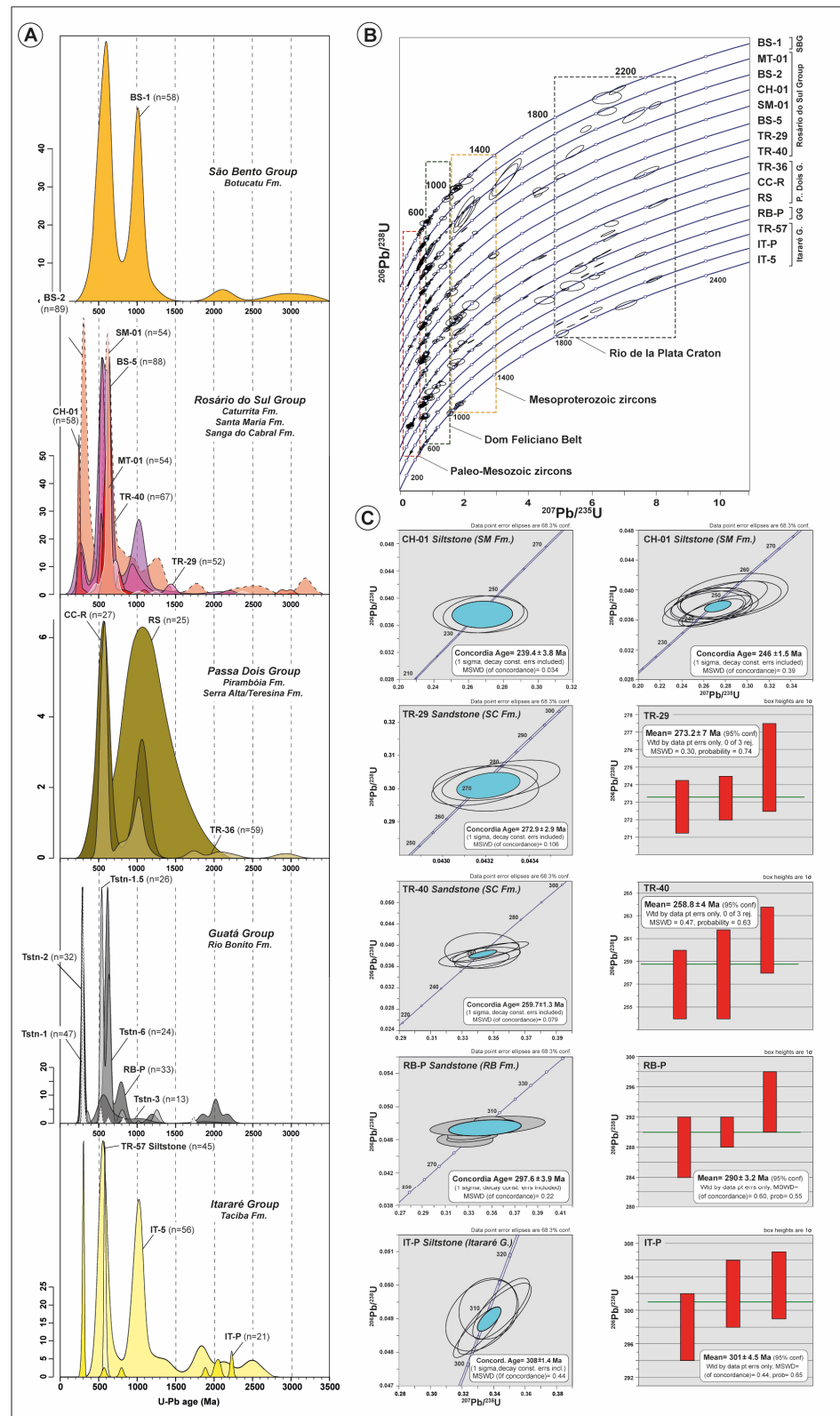


Figure 6. (A) Integrated kernel probability density plot (KDP) diagram for detrital zircon from the analyzed samples from the stratigraphic units of the southern sector of the Paraná Basin. (B) Comparative Concordia diagrams of the analyzed samples, illustrating the relationships between the main concentrations of zircon results. (C) Concordia diagrams and weighted average ages for the ash fall zircons.

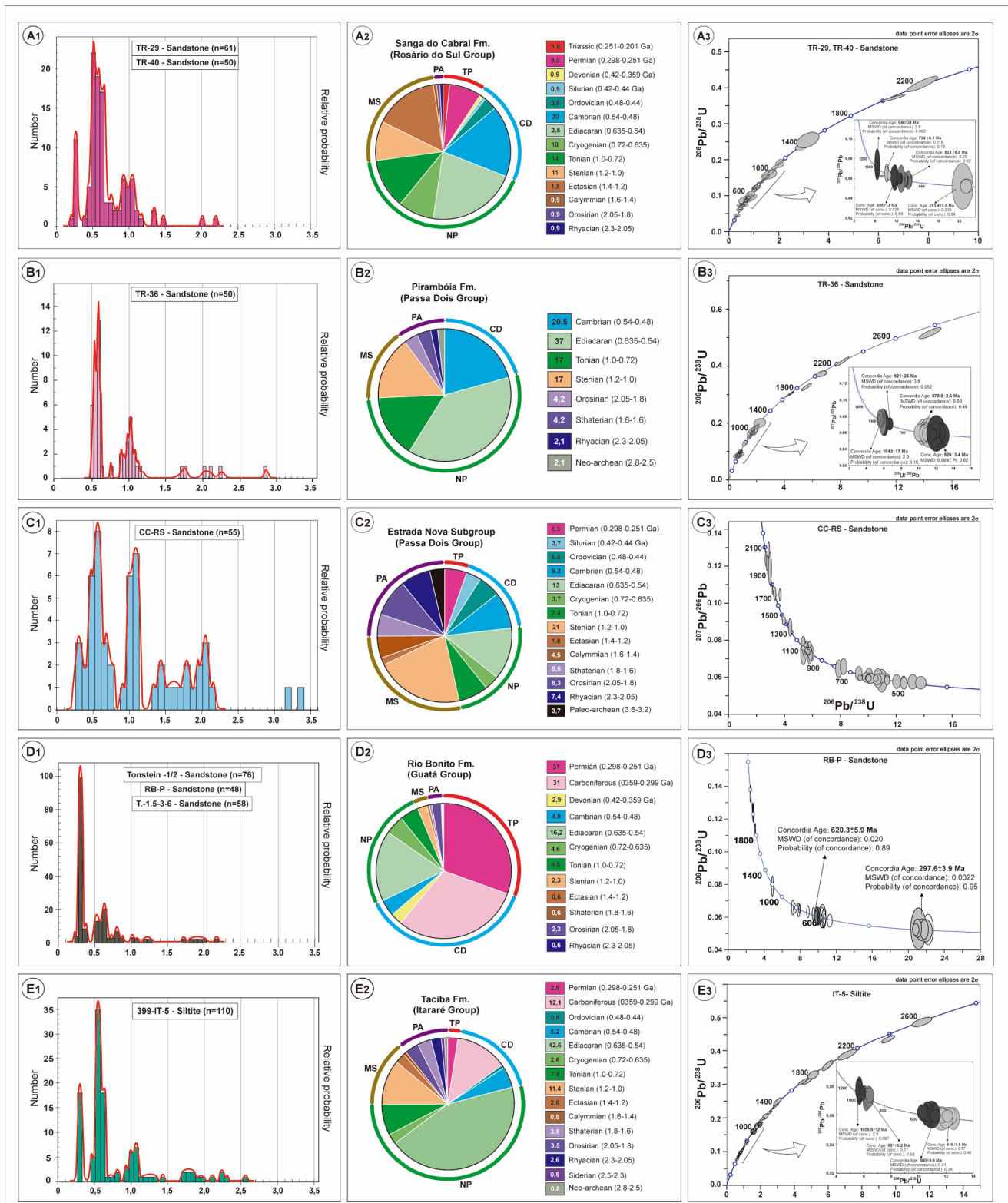


Figure 7. (1) Probability density plot (PDP) diagrams, (2) pie chart graphics showing the proportion of the zircon ages according to the periods in the chronostratigraphic chart, and (3) Concordia diagrams displaying ages from the main zircon populations in the analyzed samples. Lithostratigraphic formations: (A) Sanga do Cabral (Rosário do Sul Group), (B) Pirambóia, (C) Palermo (Passa Dois Group), (D) Rio Bonito (Guatá Group) and (E) Taciba (Itaré Group).

The sample Tnst-6 provided 23 zircons, from which 16 were used to calculate the age of the youngest population associated with an ash fall layer. The youngest population comprise prismatic, euhedral, and elongated crystals with bipyramidal terminations and well-defined oscillatory zoning. The crystals range in size from 120 to 340 μm , and the L:W ratio varies from 4:1 to 12:1. The subordinate detrital grains comprised sub-euhedral crystals with pyramidal terminations and sub-rounded shapes, both with well-defined oscillatory zonation. The sizes range between 40 and 100 μm and the L:W ratio varies from 1:1 to 5.1. The crystals are considered to be of igneous origin, with Th/U ratios ranging between 0.26 and 1.79. The results presented $^{238}\text{U}/^{206}\text{Pb}$ ages ranging from 289 to 306 Ma. The volcanic zircons yielded a Concordia age of 300.1 ± 1.2 Ma (MSWD = 0.22, n = 16) and 301.5 ± 1.3 Ma (MSWD = 0.67, n = 12). The subordinate detrital zircons showed Paleozoic ages between 319 and 321 Ma, and an older population with ages of 535–531 Ma, 631 Ma, 828 Ma, and 1.741 Ma (Figures 6A and 7D1, and Table S6).

In total, 71 zircon grains from the fine-grained sandstone of sample RB-P were analyzed, from which 38 showed concordant results (Table S7). This sample was associated with the Tnst-1 and Tsnt-2 ash fall levels. The results revealed two $^{238}\text{U}/^{206}\text{Pb}$ age populations. A main detrital group with 26 grains showed Pre-Cambrian ages between 512 and 2170 Ma, and a subordinate Paleozoic population with 12 grains of volcanic origin with ages ranging from 219 Ma to 367 Ma (Figures 6A and 7D1,D2). The grain size ranges from 77 to 292 μm . The Th/U ratios show values that vary between 0.32 and 1.76, interpreted as igneous crystals. $^{238}\text{U}/^{206}\text{Pb}$ ages range from 288 to 303 Ma. The volcanic zircons yielded a Concordia age of 297.6 ± 3.9 Ma (MSWD = 0.22, n = 6) and the three youngest zircons yielded a weighted average age of 290 ± 3.2 Ma (MSWD = 0.55, n = 3) (Figure 6). The radiometric ages of all samples range from 297 up to 301.5 Ma, indicating a deposition in the Carboniferous–Permian interval, between Ghzelian and Asselian, in the lower interval of post-glacial deposits.

4.2. Passa Dois Group

4.2.1. Teresina Formation

The sample CC-R is a brown shale collected at Cerro das Caveiras, north of Dom Pedrito city (Figure 4). In total, 80 zircons were analyzed, from which 61 yielded concordant results (Table S8). Most of the zircons showed Paleozoic and Neoproterozoic ages (Figures 6A and 7C1). The euhedral zircon crystals have prismatic and elongated shapes with pyramidal terminations and well-defined oscillatory zoning. The sizes range from 80 to 120 μm and the L:W ratio varies from 3:1 to 7:1. The oldest detrital population is constituted by prismatic to elliptical, rounded to sub-rounded grains. The sizes vary between 40 and 70 μm and the L:W ratio varies from 1:1 to 2.1.

The detrital zircons feature a wide range of ages between 269 and 3346 Ma (Figure 7C2). The Paleozoic grains show $^{238}\text{U}/^{206}\text{Pb}$ ages ranging from the Permian (284–269 Ma), Silurian (428–420 Ma), Ordovician (488–482 Ma) and Cambrian (540–518 Ma) (Figure 7C3). The Neoproterozoic zircons have Ediacaran (595–567 Ma), Cryogenian (637 Ma), and Tonian (990–892 Ma) ages. The Mesoproterozoic grains yielded Stenian (1115–1018 Ma) and Calymmian (1430–1382 Ma) ages, while the Paleoproterozoic zircons showed Statherian (1633 Ma) and Orosirian (2065–2004 Ma) ages. The oldest grains belong to the Paleoproterozoic, with ages between 3434 and 3404 Ma.

4.2.2. Pirambóia Formation

The sample TR-36 is a pink, medium-grained, well-sorted arkosic sandstone with cross-stratification and low-angle, planar cross-stratification, collected near Rosário do Sul town (Figure 4). Out of the 70 detrital zircons analyzed, 58 presented concordant analyses, from which 9 distinct populations of ages could be recognized (Table S9). The grains have a rounded shape and vary in size from 80 to 350 μm . The dominant Neoproterozoic zircon crystals have prismatic, elongated, and euhedral shapes with pyramidal terminations. The grain size ranges from 120 to 350 μm , with the L:W ratio varying from 4:1 to 8:1. The

subordinate Carboniferous zircons present prismatic and euhedral shapes with pyramidal terminations. The Th/U ratios are typical of magmatic crystals, ranging between 0.20 and 2.13, with one grain having a ratio of 0.05.

Two main Neoproterozoic age peaks are present, with $^{238}\text{U}/^{206}\text{Pb}$ ages ranging from 623–539 Ma to 986–751 Ma (Figures 6A and 7B1). The subordinate peaks showed Carboniferous ages between 536 and 491 Ma and Mesoproterozoic ages from 1120 to 1014 Ma (Figure 7B2). A few grains yielded $^{207}\text{Pb}/^{206}\text{Pb}$ ages between 2850 and 1713 Ma. Four reference ages representative of the main age peaks were determined through Concordia (Wetherill) ages of 1047 ± 12 Ma (MSWD = 2.0, $n = 7$), 921 ± 26 Ma (MSWD = 3.8, $n = 6$), 576 ± 3 Ma (MSWD = 0.50, $n = 16$), and 526 ± 3 Ma (MSWD = 0.0097, $n = 13$) (Figure 7B3). Other subordinate peaks showed ages between 623–604, 794–751, 898–890, 1753–1713, 2012, 2250–2090, and 2850 Ma.

4.3. Rosário do Sul Group

4.3.1. Sanga do Cabral Formation

The samples TR-29 and TR-40 are sandstones from the base of the Rosário do Sul Group. The TR-40 is a light pink, medium-grained arkosic sandstone with cross- and plane-parallel stratification, collected in a road cut of BR-474 highway, near Rio Pardo city (Figure 4). A total of 86 zircon grains yielded 66 concordant results (Table S10). Seven crystals showed elongated and euhedral prismatic shapes and well-defined oscillatory zoning, indicating a volcanic origin associated with ash fall layers. The crystals vary between 100 and 120 μm in length, with the L:W ratio ranging from 4:1 to 8:1. The other 59 grains are detrital, with a main group consisting of zircons with prismatic, elongated, and euhedral shapes, pyramidal terminations, and rounded edges. A subgroup is defined by rounded to ovoid shapes. Grain sizes vary between 70–120 μm , with a L:W ratio ranging from 2:1 to 4:1. The Th/U ratios range between 0.13 and 1.56, indicating magmatic crystals. Six main age peaks from 251 Ma to 2070 Ma were recognized, including two Neoproterozoic peaks with subordinate Mesoproterozoic ages (Figures 6A and 7A1). The main interval shows $^{206}\text{Pb}/^{238}\text{U}$ ages varying from 535–469 Ma, 613–545 Ma, 696–629 Ma, and 995–792 Ma, to 1167–1004 Ma (Figure 7A2). U-Pb isotopic data from the youngest zircon with volcanic origin yielded a $^{206}\text{Pb}/^{238}\text{U}$ weighted average age between 260 ± 3 Ma (MSWD = 0.30, $n = 6$) and 257 ± 9 Ma (MSWD = 0.32, $n = 4$), suggesting the maximum time interval of deposition (Figures 6C and 7A3).

The sample TR-29 is a pink, medium-grained arkosic sandstone with cross-bedding stratification collected between the cities of São Francisco de Assis and São Vicente (Figure 4). The analysis of 69 zircon grains produced 53 concordant results (Table S11). Most of the zircons have prismatic, elongated, and euhedral shapes with pyramidal terminations and well-defined oscillatory zoning, with a subordinate population of crystals with rounded edges. The sizes vary from 80 to 120 μm , and with a L:W ratio varying from 3:1 to 6:1.

The oldest grains have an ovoid shape and sizes between 50 μm and 90 μm . A wide age interval varying from 245 Ma to 2188 Ma was observed (Figures 6A and 7A2). Concordia (Wetherill) determined four main peaks: 946 ± 31 Ma (MSWD = 2.8, $n = 4$), 734 ± 6 Ma (MSWD = 0.11, $n = 3$), 595.6 ± 13 Ma (MSWD = 0.024, $n = 9$) and 533 ± 7 Ma (MSWD = 0.25, $n = 18$). Other subordinate peaks were characterized by $^{207}\text{Pb}/^{206}\text{Pb}$ ages between 1443–1016 Ma and 2188 Ma. The Paleozoic crystals are dominant and show two main peaks ranging from 280–245 Ma, to 535–365 Ma. Neoproterozoic ages are subordinated, having three main age intervals of 620–545 Ma, 709–634 Ma, and 982–734 Ma. The youngest prismatic and euhedral crystals, interpreted as Permian detrital zircons of volcanic origin, yielded a Concordia age of 273 ± 4 Ma (MSWD = 0.038, $n = 4$), like the $^{206}\text{Pb}/^{238}\text{U}$ weighted average age of 273.8 ± 6 Ma (MSWD = 0.23, $n = 4$) (Figures 6C and 7A3).

4.3.2. Santa Maria Formation

A total of 291 zircons from the samples BS-5 and SM-01 are from sandstones of the basal portion of the Santa Maria Fm. (Passo das Tropas Member, sensu [19]), and from the

samples BS-2 and CH-01, which are siltstones from the upper portion (Alemoa Member, sensu [19], or Santa Cruz Sequence sensu [16]) (Figure 4). The data from the samples BS-2 and BS-5 were published by [15].

The sample BS-5 is a pink, well-sorted, fine-grained sandstone. The 87 concordant zircons yielded a narrow Neoproterozoic $^{206}\text{Pb}/^{238}\text{U}$ age range, from 833 to 569 Ma, with three representative age peaks within the dominant intervals of 620–559 Ma, 709–622 Ma, and 833–750 Ma (Figures 6A and 8D1). The Th/U ratios vary from 0.1 and 1.32, suggesting a magmatic origin.

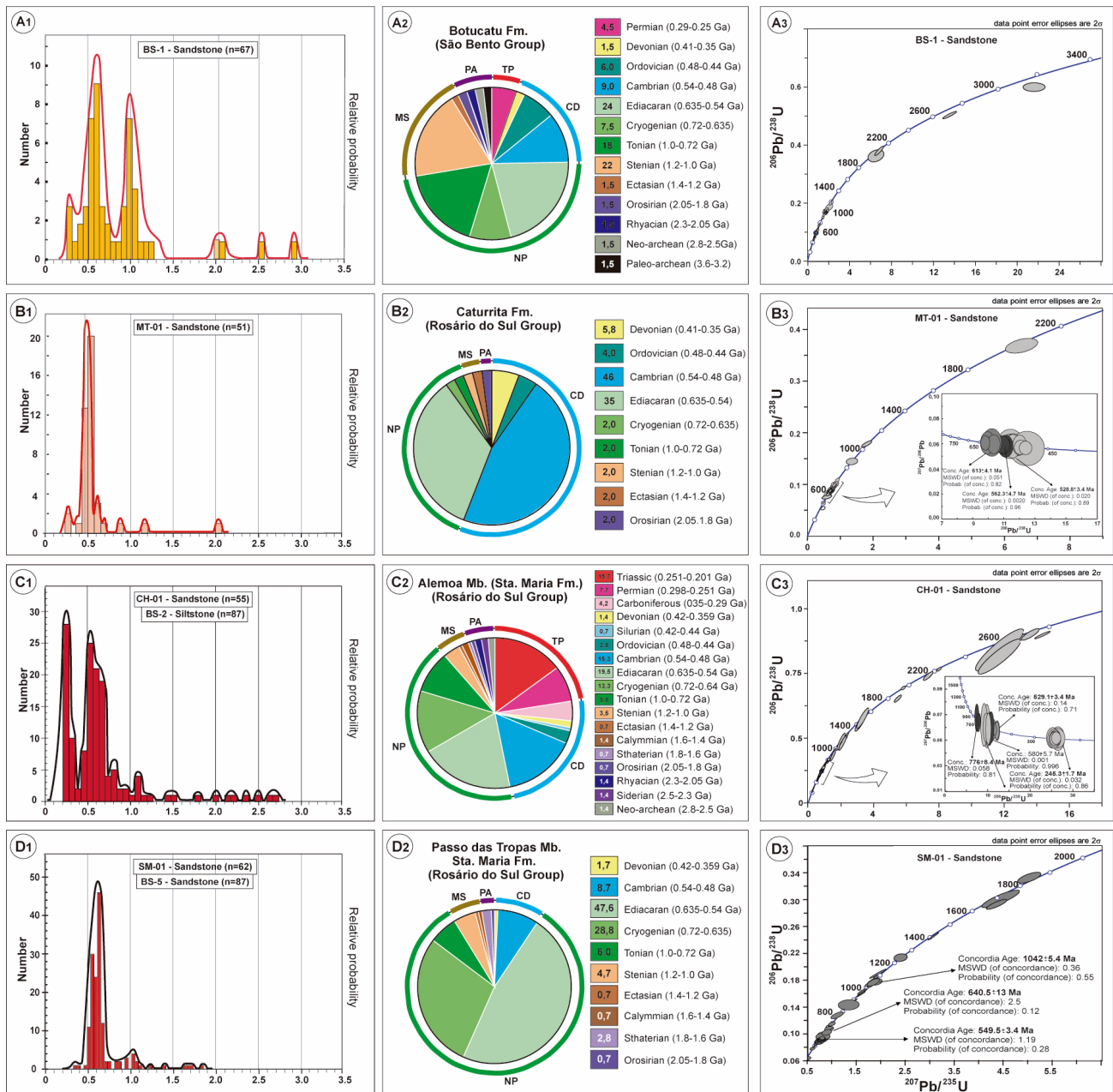


Figure 8. (1) Probability density plot (PDP) diagrams, (2) pie chart graphics showing the proportion of the zircon ages according to the periods in the chronostratigraphic chart, and (3) Concordia diagrams showing ages from the main zircon populations in the analyzed samples from the stratigraphic units of the southern sector of PB. Lithostratigraphic formations: (A) Botucatu (São Bento Group), (B) Caturrita (Rosário do Sul Group), (C) Santa Maria, Alemoa Member (Samples BS-2, PT-SM) and (D) Santa Maria, Passo das Tropas Mb (Samples BS-5, PT-SM).

The sample SM-01, collected near to Santa Maria city, is a pink, cross-bedded, medium-grained sandstone. The 63 concordant zircons yielded a large age range from 357 Ma to 1850 Ma, with dominant ages between 620 and 541 Ma (Figure 8D1, Table S12). The Paleozoic zircons showed ages varying between 538 and 357 Ma, with an expressive population of Cambrian age (538–503 Ma) (Figure 8D3). Subordinate Neoproterozoic $^{206}\text{Pb}/^{238}\text{U}$ ages range from 700–645 Ma to 972–773 Ma, along with grains recording Mesoproterozoic ages from 1247 to 1026 Ma, and restricted Paleoproterozoic ages in the 1850–1665 Ma range. The Th/U ranges between 0.18 and 1.88. Three main groups of zircon grains were defined by U-Pb Concordia ages of 550 ± 3 Ma, 641 ± 13 Ma, and 1042 ± 5 Ma. Others age peaks are spread from 357 ± 4 Ma and 1800 ± 38 Ma.

Sample BS-2 corresponds to a red siltite collected in Venâncio Aires city (Figure 4). Most of the zircon grains are generally rounded; however, a small population of euhedral and elongated prismatic crystals occurs. The Th/U varies between 0.09 and 0.18, indicating an igneous origin. The 92 concordant grains yielded a wide range of ages from 217 Ma to 2742 Ma. The abundant Paleozoic zircons include six main age peaks: 249–217 Ma, 286–251 Ma, 350–300 Ma, 361–356 Ma, 496–470 Ma, and 536–502 Ma (Figures 6A and 8C1). Subordinate Archean to Mesoproterozoic age intervals showed peaks of 2742–2681 Ma, 2225–1913 Ma, 1517–1500 Ma, and 1231–1041 Ma. Neoproterozoic zircons show two main age intervals of 999–743 Ma and 718–653 Ma.

A small population of crystals with euhedral and elongated prismatic shapes is interpreted as being of volcanic origin. The Th/U ranges from 0.89 to 1.94. Out of six crystals, five yielded ages between 240 and 232 Ma, and the $^{206}\text{Pb}/^{238}\text{U}$ weighted average age of 237 ± 2 Ma is interpreted as the best estimate for the crystallization of the volcanic ash and the maximum depositional age of the top of the Santa Maria Formation [15]. Another population of volcanic zircons yields a U-Pb Concordia age of 246 Ma. The Mesoproterozoic and Paleoproterozoic zircons are rounded, suggesting transportation over long distances and/or multiple sedimentary cycles. On the other hand, the Paleozoic zircons are elongated and euhedral, suggesting transportation over short distances. Two populations of zircon grains populations are composed of euhedral zircons with long prismatic shapes, indicating a close source area and a probable volcanic origin.

The sample CH-01 is a siltite of the Alemoa Member collected to the north of the Cachoeira do Sul city (Figure 4). We identified three distinct groups of zircon grains. The crystals come with concentric oscillatory zoning, which is a typical feature of primary magmatic zircon [57]. The Paleoproterozoic zircon crystals are sub-euhedral, with prismatic and elongated shapes, as well as round grains. The Neoproterozoic zircon crystals also exhibit elongated and euhedral shapes, suggesting transportation over short distances. The youngest crystals, interpreted as originating from volcanic ash, have euhedral forms with long prismatic shapes, indicating a close source area and probable volcanic origin. Most of the zircons are sub-euhedral, with prismatic elongated and bipyramidal shapes, featuring sub-rounded faces. The sizes range from 90 to 250 μm in length, with L:W ratios ranging from 2:1 to 4:1. Another subgroup consists of grains with prismatic shapes and rounded edges, exhibiting ovoid or round forms and sizes varying between 200 and 300 μm .

The youngest crystals have euhedral and elongated prismatic shapes, with sizes ranging from 200 to 650 μm , mostly around 400 μm in length. The Th/U ranges from 0.76 to 1.22. Fifty-six (56) concordant zircon grains yielded ages ranging from 239 to 2630 Ma (Table S13). Six zircon populations are defined by age intervals of 249–239 Ma, 293–251 Ma, 535–509 Ma, 620–541 Ma, 669–623 Ma and 813–759 Ma (Figures 6A and 8C1,C2). Four groups are defined based on U-Pb Concordia ages of 529 ± 4 Ma, 580 ± 6 Ma, 640 ± 3 Ma, and 776 ± 8 Ma. The youngest zircon crystals yielded $^{206}\text{Pb}/^{238}\text{U}$ ages between 239 and 251 Ma. The Concordia age of 246 ± 1.5 Ma (MSWD = 0.39, $n = 8$) and the $^{238}\text{U}/^{206}\text{Pb}$ weighted average age of 239.4 ± 3.8 Ma (MSWD = 0.034, $n = 2$) are interpreted as the crystallization of the volcanic ash and the maximum depositional age of the Alemoa Member (Figures 6C and 8C3).

4.3.3. Caturrita Formation

The sample MT-01 is a cross-bedded, medium-grained arkosic sandstone collected near Mata town, corresponding to the upper portion of the Rosário do Sul Group (Figure 4). A total of 53 zircon grains produced 33 concordant results (Table S14). Most of the zircons have euhedral to sub-euhedral prismatic elongated shapes with pyramidal terminations, rounded edges, and well-defined oscillatory and sector zoning. The sizes vary from 80 to 500 μm , and the L:W ratio ranges from 3:1 to 7:1. The oldest group of zircons has a rounded to ovoid shape and sizes between 50 and 90 μm . Most of these grains show homogeneous and bright internal areas typical of metamorphic zircon. The Th/U ranges from 0.18 to 1.28 and is representative of igneous zircons. Two age peaks were recognized to be in a wide-range interval from 365 Ma to 2074 Ma (Figures 6A and 8B1,B2). The majority of zircons show Paleozoic ages from the Cambrian (537–497 Ma), Ordovician (473–470 Ma) and Devonian (406–365 Ma) periods. The subordinate group has Neoproterozoic ages from Ediacaran (629–542 Ma) to Tonian (869–662 Ma) with single Mesoproterozoic (1056 Ma) and Paleoproterozoic (2074 Ma) ages. Three main peaks were defined by Concordia (Wetherill) ages of 617.4 ± 4.4 Ma (MSWD = 0.41, n = 5), 562.3 ± 4.7 Ma (MSWD = 0.0020, n = 4) and 528.8 ± 3.4 Ma (MSWD = 0.020, n = 12) (Figure 8B3).

4.4. São Bento Group

Botucatu Formation

The sample BS-1 is an aeolian, medium-grained quartz-rich subarkosic sandstone with large-scale cross-bedding stratification representing the base of the Botucatu Formation in the upper portion of the São Bento Group (Figure 8). A total of 78 zircon grains were analyzed, of which 57 were concordant (Table S15). Three crystals with euhedral elongated prismatic shapes and rounded edges, ranging in size between 250–500 μm long and with a L:W ratio ranging from 3:1 to 6:1, are interpreted as reworked grains from the ash fall layer. The other 54 grains are detrital, with the main group consisting of grains with euhedral and prismatic elongated shapes, with pyramidal terminations, and rounded to very rounded edges. The other subgroup shows a rounded to ovoid shape. The sizes vary between 70 and 120 μm , and the L:W ratio ranges from 2:1 to 4:1. The Th/U ranges between 0.16 and 2.60, representing igneous crystals, supported by well-defined oscillatory zoning.

Four main age peaks were defined in the wide interval from 262 Ma to 3291 Ma (Figures 6A and 8A1). Two Neoproterozoic peaks were found in the Ediacaran (638–561 Ma) and Tonian (995–741 Ma), with subordinate ages from the Cryogenian (683–647 Ma). Mesoproterozoic zircons range from 1220 to 1005 Ma. The Paleozoic grains include subordinate ages from Permian (279–262 Ma), Devonian (379 Ma), Ordovician (469–446 Ma), and Cambrian (536–499 Ma). Paleoproterozoic (2107–2102 Ma) and Archean (3291 to 2790 Ma) (Figure 8). Isotopic data from the youngest zircons with volcanic origin yielded a Concordia age of 264.2 ± 3.8 Ma (MSWD = 0.0020, n = 2) and a $^{206}\text{Pb}/^{238}\text{U}$ weighted average age of 264 ± 7.5 Ma, (MSDW = 0.41, n = 2). The volcanic crystals have rounded edges, suggesting a reworking process of the original ash fall.

5. Discussion

5.1. Provenance of Detrital Zircon

The U-Pb ages, integrated with sedimentary paleo-transport data from the southern Paraná Basin (PB), indicate provenance from short and long distances located at the south, southeast, and southwest of the basin limits. The analyses of samples representative of the five groups of the PB show a wide range of age populations that are present in all units (Figures 6–9) and a strong correlation with local and distal source areas.

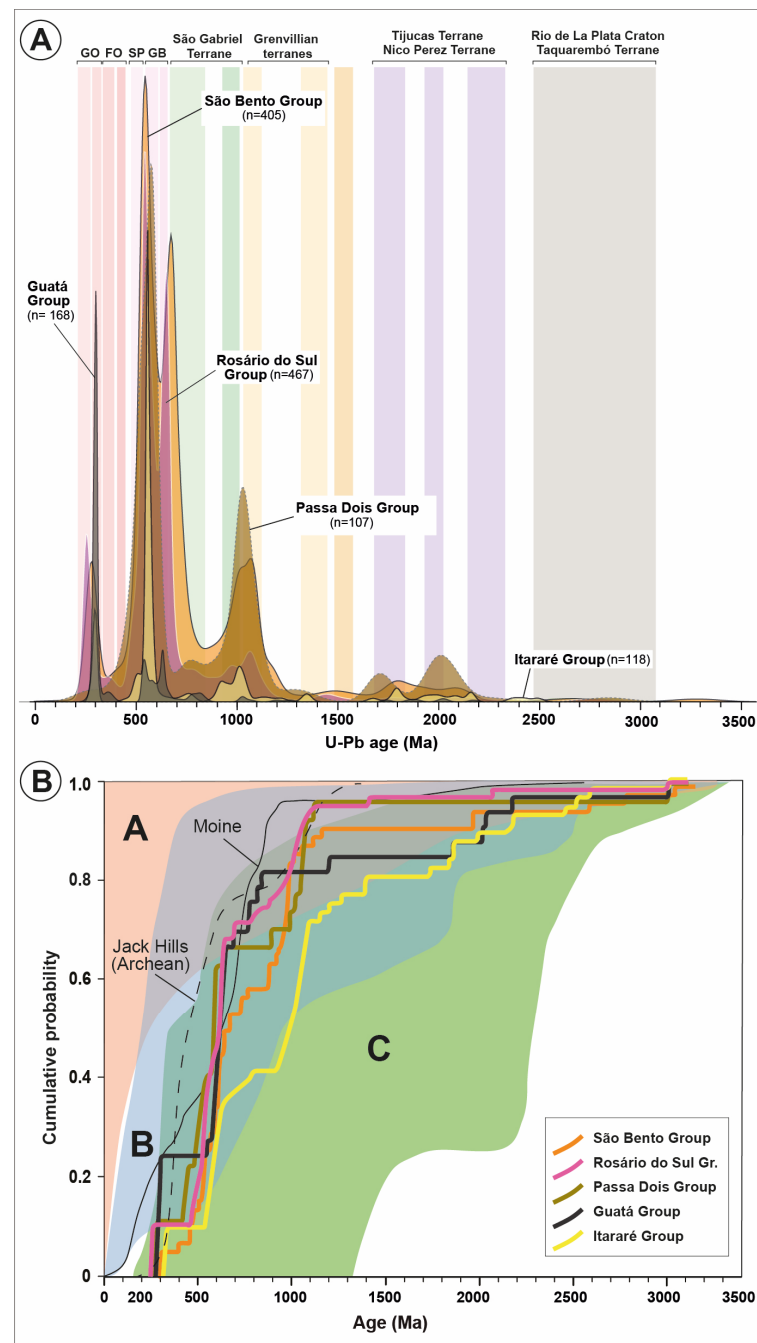


Figure 9. (A) Integrated kernel probability density plot (KDP) diagram for detrital zircon from the stratigraphic units of the southern sector of the Paraná Basin. The shaded background fields represent tectonic/orogenic events. Batholiths: AB—Aiguá; PB—Pelotas. Orogenies: FO—Famatinian; GO—Gondwanides; SP—Sierras Pampeanas. (B) Cumulative probability plot (CAD) diagram for the same samples plotted using Isoplot-R-based provenance software (Vermeesch et al., 2018) [49]. Stratigraphic ages are based on the maximum depositional age of individual groups of samples. The shaded general fields for convergent (A: pink), collisional (B: blue) and extensional basins (C: green) were determined by Cawood et al. (2012) [10]. The fields were proposed based on the differences between the crystallization and depositional ages (CA-DA) of the zircons. Extensional (including intracratonic) settings have CA-DA > 150 Ma in the youngest 5% of the zircons, and all convergent settings have CA-DA < 100 Ma in the youngest 30% of zircons. Solid and dashed lines represent patterns of CA-DA for a series of structurally disrupted and metamorphosed Precambrian sedimentary successions (i.e., Jack Hills and Moine successions).

The following main age populations and their respective source areas are considered in this work: (i) Archean to Paleoproterozoic ages from the Rio de La Plata Craton and Taquarembó Terrane to the south; (ii) Mesoproterozoic grains potentially sourced from the Grenvillian basement of the Gondwanides belt in Argentina to the southwest, and the Namaqua-Natal belt in Africa; (iii) Neoproterozoic ages from the Brasiliano–Pan-African Orogeny, with a major contribution from the Dom Feliciano Belt; and (iv) Paleozoic populations from orogenic belts in Argentina and eroded units of the Paraná Basin (Figure 10). We highlight the dominant occurrence of Neoproterozoic (996–538 Ma) and Paleo-Mesozoic (520–236 Ma) grains, with subordinate Mesoproterozoic crystals (1.2–1.0 Ga) followed by Paleoproterozoic grains. Although zircons with Paleoproterozoic and Archean ages are less common, these sources were available throughout the basin’s sedimentation, persisting for the entire section of the PB. Only the samples from the Rio Bonito Formation do not contain Archean zircons, with most of the analysis focusing on euhedral crystals related to the ash fall layers representing the depositional ages.

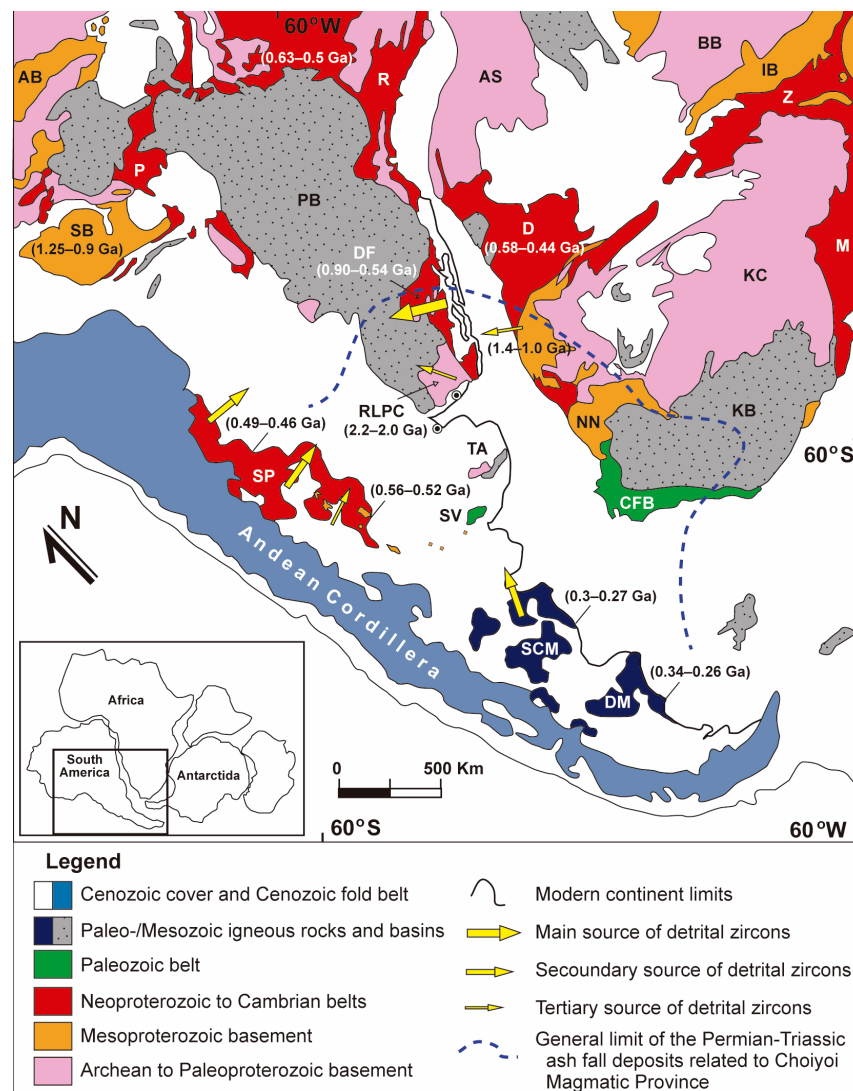


Figure 10. Provenance of the Paraná Basin formations in Rio Grande do Sul (RS) based on sedimentary transport directions and detrital zircon U-Pb ages. Comparative U-Pb data from [58–68]. Cratons: AS—Angolan Shield, DM—Deseado Massif, KC—Kalahari, and SCM—Samancor Massif. Orogenic belts: AB—Aguapeí, BB—Bangweulu, CFB—Cape Fold Belt, D—Damara, DF—Dom Feliciano, IB—Irumide, MB—Mozambique, NN—Namaqua-Natal, PBA—Paraguay-Araguaia, R—Ribeira, SB—Sunsás, SP—Sierras Pampeanas, SV—Sierra de la Ventana, and ZB—Zambezi. Basins: PB—Paraná Basin, and KB—Karoo Basin. Modified from [69].

The Itararé Group (samples IT-5, IT-P, and TR-57) presented six main detrital zircon populations: Neoproterozoic (2.5 Ga), Lower to Mid-Paleoproterozoic (2.3–2.1 and 2.0–1.8 Ga), Grenvillian (1.2–1.0 Ga), Brasiliano I (996–747 Ma), Brasiliano II (640–537 Ma) and Paleozoic (519–291 Ma) (Figure 9A). The exception is sample TR-57, which shows only Neoproterozoic zircons from the Ediacaran period (610–564 Ma). The Neoproterozoic ages are dominant, followed by Paleozoic zircons, with a majority of Cambrian and Carboniferous grains, as well as Paleo-Mesoproterozoic populations.

The overlying Guatá Group is dominated by Paleozoic and Neoproterozoic ages (840 and 542 Ma, with a main peak in 600–550 Ma), with subordinate Mesoproterozoic (1.2–1.0 Ga) zircons. Paleozoic grains show two main age periods, 534–345 Ma and 316–284 Ma. The data show a less significant Paleoproterozoic (2.3–1.8 Ga) grain population and a higher contribution of Paleozoic detrital zircons compared to those for the Itararé Group (Figure 7D2). The Paleozoic grains are dominated by Carboniferous and Permian ages. This abrupt increase in the Paleozoic zircon population could be explained by the onset of the diastrophism of the Gondwanan Orogeny during the Sanrafaelic Orogenic Phase [2] in the transition from the Itararé to Guatá Group. This compressional phase generated intense deformation through folding and thrusting followed by the resumption of southward subduction.

The analyses of the Upper Permian Passa Dois Group units show a similar range of ages to those observed in the underlying Itararé and Guatá Groups. However, they exhibit a higher proportion of Archean-Proterozoic populations. Two peaks of Mesoproterozoic (1328–1008 Ma) and Neoproterozoic (623–539 Ma) ages are present, with rare Archean grains (3436–2850 Ma). The Paleozoic zircons are subordinate and exhibit ages ranging from 534 to 269 Ma. This period is characterized by the continuous uplift of the Gondwanides Belt during the Sanrafaelic Phase, resulting from the subduction of the Panthalassa oceanic plates beneath the Gondwana continent. The paleocurrents indicate predominant sedimentary transport to the north and northwest, suggesting that the Paleozoic zircons can be associated with the Famatinian Terrane to the west-southwest and the Somuncurá Massif in northern Patagonia (Figure 10). The sediments supplied by these distant sources were transported by transcontinental alluvial and fluvial systems, crossing the Ventania Fold Belt and related foreland deposits, and subsequently forming peripheral bulges before being deposited in the intracratonic realm. This paleogeographic relationship is also described by [69] for the paleogeographic analysis of Late Permian rocks in the Rio do Rasto Formation in the states of Rio Grande do Sul and Santa Catarina.

Further up in the succession, the detrital zircon patterns recorded in Triassic samples from the Rosário do Sul Group show a broad spectrum of source rocks, with ages ranging from the Meso-Archaean to the Meso-Triassic. Three main age groups are defined: (1) a group with two dominant populations from the Neoproterozoic, with emphasis on the Cryogenian and Ediacaran intervals (700–500 Ma), (2) one with two populations from the Middle–Upper Paleozoic (450–250 Ma), and (3) another with an early Mesozoic group of zircons. Subordinate groups include Mesoproterozoic zircons (1500–1231 Ma and 1231–1041 Ma), and Neoproterozoic zircons from the Tonian to Cryogenian (1000–669 Ma). The contribution of ancient sources is restricted, with few Archean (2881–2681 Ma) and Paleoproterozoic (2225–2052 Ma, 1913–1900 Ma, and 1800–1517 Ma) grains.

The uppermost Jurassic–Cretaceous São Bento Group shows age peaks ranging from 262 Ma to 3291 Ma. Two subordinated Archean ages (3291 to 2790 Ma) and Paleoproterozoic ages (2107–2102 Ma) were shown, with Mesoproterozoic zircons varying from 1220 to 1005 Ma. A main Neoproterozoic group with peaks in the Ediacaran (638–561 Ma), Tonian (995–741 Ma), and subordinate Cryogenian (683–647 Ma) ages was identified, along with a Paleozoic peak including ages from the Permian (279–262 Ma), Devonian (379 Ma), Ordovician (469–446 Ma) and Cambrian (536–499 Ma).

5.1.1. Pre-Cambrian Sources

The sedimentary strata in the southern sector of the PB were deposited along the border of the Rio de la Plata and Luis Alves cratons, overlying the Nico Perez Terrane and Dom Feliciano Belt (Mantiqueira Province) [70–72] (Figures 1 and 3). The basement is characterized by large Archean–Paleoproterozoic cratonic units, surrounded by Neoproterozoic orogenic belts formed during the Brasiliano Orogenic Cycle (900–540 Ma) [38]. Towards the southwest, the Rio de La Plata Craton is surrounded by the Paleozoic Pampean, Famatinian, and Gondwanic [18,73]. In southern Brazil and Uruguay, most of the tectonic contacts between orogenic units exhibit a dominant NE–SW orientation marked by ductile shear zones or extensional fracture zones generated during the main collisional stage of the Brasiliano Cycle (~650–620 Ma) [35,72]. The reactivation of older basement structures has been attributed to the action of compressive stresses associated with the Paleozoic orogenesis in SW Gondwana and subsequent reactivation linked to the breakup of Gondwana during the Cretaceous [2,15,36,37].

The sedimentary rocks in the southern sector of the PB are exposed as an elongated zone of an E–W and N–S outcrop belt, surrounded by Precambrian basement rocks exposed along the south and southeast margins of the PB (Figure 4). The Precambrian sources are interpreted to have been mainly derived from units of the Rio de La Plata Craton, represented by the Taquarembó Terrane in Brazil, the Nico Peres Terrane in Uruguay, and the Dom Feliciano Belt (São Gabriel, Tijucas, and Punta del Este terranes, and Florianópolis–Pelotas–Aiguá batholiths) (Figure 3). These units are bounded by regional shear zones of NE–SW and subordinate NW–SE directions. The Mesoproterozoic grain populations can be related to the distal sources, associated with the basement of the Gondwanides Belt in Argentina and Chile, as well as the Namaqua–Natal belt providing Grenvillian zircons.

The Archean–Neoproterozoic metamorphic and granitic rocks of the southern Brazil and Uruguay have two major provenance time intervals: an older one ranging from 3.1 to 1.7 Ga and a younger one from 900 to 540 Ma, with minor Mesoproterozoic ages [15,71,72,74,75]. The Taquarembó Terrane is composed of by Archean–Paleoproterozoic granulites and orthogneisses with U–Pb zircon crystallization ages ranging from 2550 to 2200 Ma, and metamorphism between 2100–2000 Ma [76], which are present in all analyzed units. The detrital Neoproterozoic zircons represent the most abundant population present in the entire succession. These zircons are interpreted as being sourced from the Brasiliano–Pan-African Cycle rocks, mainly from the local Dom Feliciano Belt (DFB). The African contribution is interpreted as limited due to the Don Feliciano High, a NE–SW positive structure that would prevent the significant advancement of African basement sources towards the northwest.

The DFB includes four arc-related magmatic associations with U–Pb crystallization ages in the intervals of 900–860 Ma (Passinho Arc), 780–720 Ma (São Gabriel and Porongos–Cerro Olivo arcs), and 650–550 Ma (Dom Feliciano Arc). The Passinho and São Gabriel arcs were related to accretionary orogenies, with a magmatism of juvenile character and mantle composition, while the magmatism of the Porongos Arc and the units of the Cerro Olivo Complex in the Punta del Este Terrane involved the generation of a Tonian magmatism associated with the reworking of a Paleoproterozoic continental crust [56,77,78].

The DFB represents the evolution of a collisional orogen, with syn-collisional peraluminous magmatism generated by crustal melting associated with high-grade orogenic metamorphism (650–620 Ma) [79,80], and a post-collisional magmatism (600–570 Ma) with a strong crustal signature [81,82]. The São Gabriel Terrane (SGT) is composed of an association of ophiolite slabs and arc-related plutonic and metavolcano-sedimentary rocks with a juvenile signature, generated between 900 and 720 Ma and interpreted as an accretionary prism [76,83–88]. The Tijucas Terrane (TjT) occurs to the east and is composed by the metavolcano-sedimentary rocks of the Porongos Complex, with volcanic activity recorded between 805–780 Ma and 600–580 Ma, and by the Paleoproterozoic orthogneisses of the Encantadas and Vigia complexes (2250–2100 Ma) [71,89,90]. The igneous and metamorphic complexes that constitute these terranes were intruded by granitic plutons (650–600 Ma) and covered by sedimentary and volcanic rocks of the Camaquã Basin

(620–540 Ma) [91,92]. The eastern portion of the DFB is composed of the Pelotas Batholith (PB), represented by granitic suites and acidic and basic dike swarms with U-Pb zircon ages between 650 and 550 Ma [72,81,82,93]. Inside of the batholith, there are basement inliers constituted by orthogneisses with U-Pb zircon ages of 2.1–2.01 Ga [94] and metagranites and orthogneisses of 780 Ma related to the Porongos Arc [70,88].

5.1.2. Paleozoic Sources

The rock sources for the abundant population of Phanerozoic grains are not found in the proximal areas in the south of Brazil. Therefore, most Paleozoic grains are interpreted to be provided by more distal sources associated with the Paleozoic belts located in the southwest Argentina and, to a lesser extent, southwest Africa (Figure 10).

The zircons of Late Paleozoic ages may have derived from different sources, including (1) the Late Paleozoic magmatic arc associated with the North Patagonian Massif in the SW Gondwana Margin, considering the paleocurrents of the Late Permian units with the main siliciclastic transport toward the north; (2) the Famatinian Terrane in the Sierras Pampeanas, considering the general E–NE paleocurrent trends for the Rosário do Sul Group (Sanga do Cabral and Santa Maria Supersequences) and the paleogeography of the Triassic succession [20,36,37,95]. Cambrian ages between 520 and 480 Ma were described in granitoids of Pampean orogeny exposed in the Sierras Pampeanas [21,22] (Figure 10). The Ordovician zircons (480–450 Ma) are described in granites and metamorphic rocks associated with the Famatinian orogeny and in the NW portion of the Sierras Pampeanas [23–25,96], as well as in the Cape Fold Belt, South Africa. Devonian age peaks (380–360 Ma) are also found from the Rio Bonito to the Botucatu formations and are likely related to intrusive granites of the Sierras Pampeanas.

Cambrian to Carboniferous zircons were transported over long distances, as suggested by the sub-rounded to rounded grain forms, whereas elongated and euhedral Permian to Triassic zircons have a volcanogenic origin and were transported by the wind as volcanic ashes (Figure 11) [15,97]. Upper Carboniferous ages were described at a tonstein layer at the top of the Taciba Formation of the Itararé Group [33]. The Permian (298–254 Ma) and Triassic (245–225 Ma) zircons are representatives of the long cycle of volcanic activities of the Choiyoi Group, located in western Argentina and southern Chile [26,41,98,99]. Permian ages have also been described in ash fall layers of tuff found in sandstones of the Rio Bonito, Irati, and Rio do Rasto formations, indicating the extent of the volcanism associated with the Gondwanides Orogeny [17,97,100–102]. In the Figure 12 we presents a synthesis of the data obtained in this work, compared which was presented by southern Brazil [97,100]. We observe the record of a greater spectrum of volcanic activity, including the volcanism that marks the end extensional period of the Gondwanides Belt, and the beginning of Andean volcanism in the Late Triassic.

The occurrence of Permian age zircons with elongated and euhedral shapes with an abraded surface in the Triassic and Jurassic rocks from the Rosário do Sul and São Bento Group, respectively, suggests a reworking of the volcanogenic zircons by the erosion of the Guatá Group and Passa Dois Group units (Figure 12B). Reworked zircons were also described in equivalent units in Santa Catarina State to the northeast of the study area [69]. These processes are associated with the uplifting of the Rio Grande Arc marked by a slow uplift of the basement throughout the Triassic and Jurassic, controlled by the Gondwanides orogeny [15,47] (Figures 1C and 14). The uplift of Permian units and the development of NW–SE regional fault systems are supported by structural characterization and apatite fission track data recording the significant uplift of the basement (~1.5 km) in the structures of the Jaguari-Mata Fault System during the Triassic [103–105].

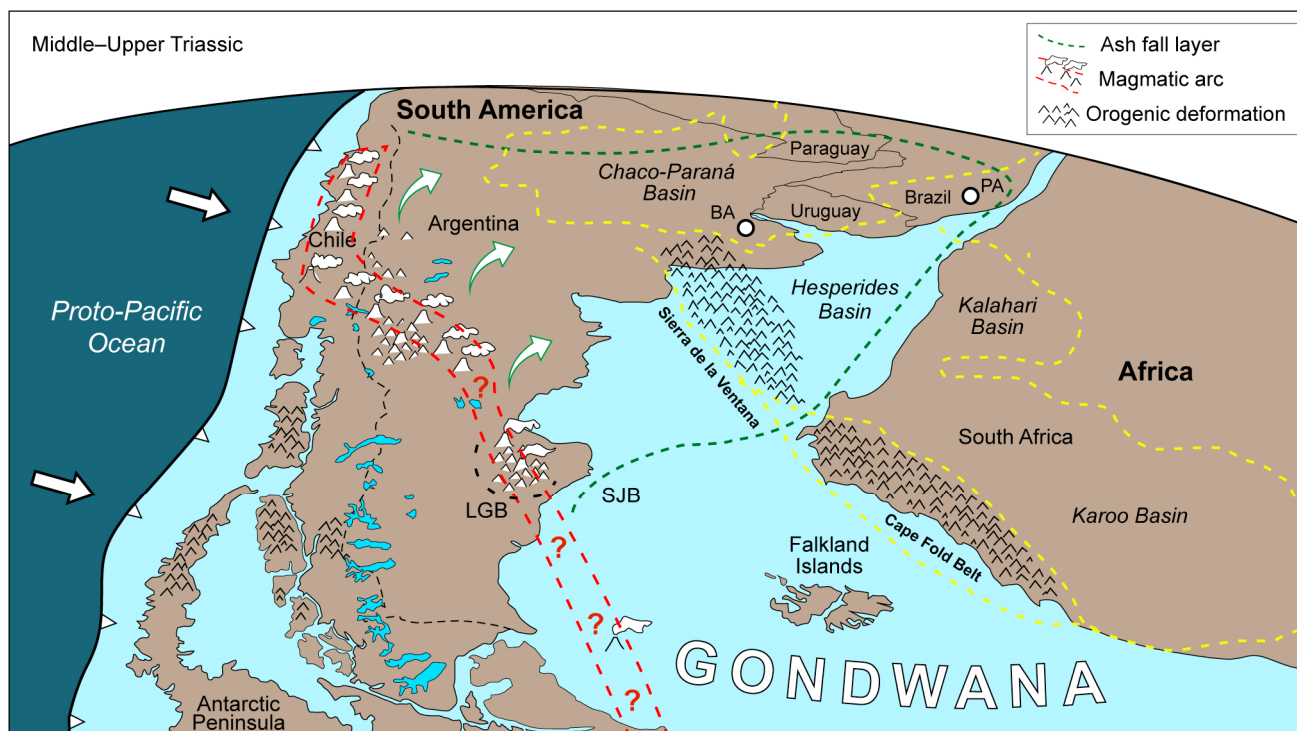


Figure 11. Location of the Middle–Upper Triassic orogenic deformation and magmatic arc in southwestern portion of the Gondwana. Paleogeographic reconstruction based on [106–108]. The yellow dashed line corresponds to the area of the Paraná, Chaco, Kalahari, and Karoo basins. Modified from [109]. The green dashed line corresponds to the general limit of the ash fall deposits associated with the Choiyoi Province magmatism.

5.2. Ash Fall Deposits and Maximum Depositional Ages

The U-Pb (LA-ICP-MS) data of volcanic zircons associated with ash fall deposits were found in sandstone and siltstone layers covering the stratigraphic sequence of the southern segment of the Paraná Basin (PB). The results were integrated with data from the Permian Rio Bonito, Irati, and Rio do Rasto formations published by [97,100], and Triassic ash fall zircons described in the southern sector of the PB by [15,47,101] (Figure 12). The volcanogenic grains provide information about the depositional ages of the Permian to Triassic units and the reworking processes of grains during the basin evolution. The data suggests volcanic activity from the Late Carboniferous to the Late Triassic, which can be associated with magmatic events of the Choiyoi Magmatism associated with the Gondwanides orogeny (Figures 2, 11 and 12).

The euhedral zircons from sample IT-P from the upper portion of the Taciba Formation (Itararé Group) yielded a Concordia age of 308 ± 1.4 Ma (MSWD = 0.44, $n = 5$) and a weighted average age of 301 ± 4.5 Ma (MSWD = 0.44, $n = 3$), suggesting this age interval as representative of the maximum depositional age. The youngest zircons from the sample RB-P from the lower portion of the Rio Bonito Formation (Guatá Group) resulted in a Concordia age of 297.6 ± 3.9 Ma (MSWD = 0.22, $n = 5$) and a weighted average age of 290 ± 3.2 Ma (MSWD = 0.60, $n = 3$), considering the maximum depositional age range. Three euhedral volcanic zircons from the ash fall layer from the Irati Formation (Passa Dois Group) showed a Concordia age of 272.9 ± 2.9 Ma (MSWD = 0.106) and a $^{238}\text{U}/^{206}\text{Pb}$ weighted average age of 273.2 ± 7 Ma (MSWD = 0.30, $n = 3$), representing the maximum depositional age.

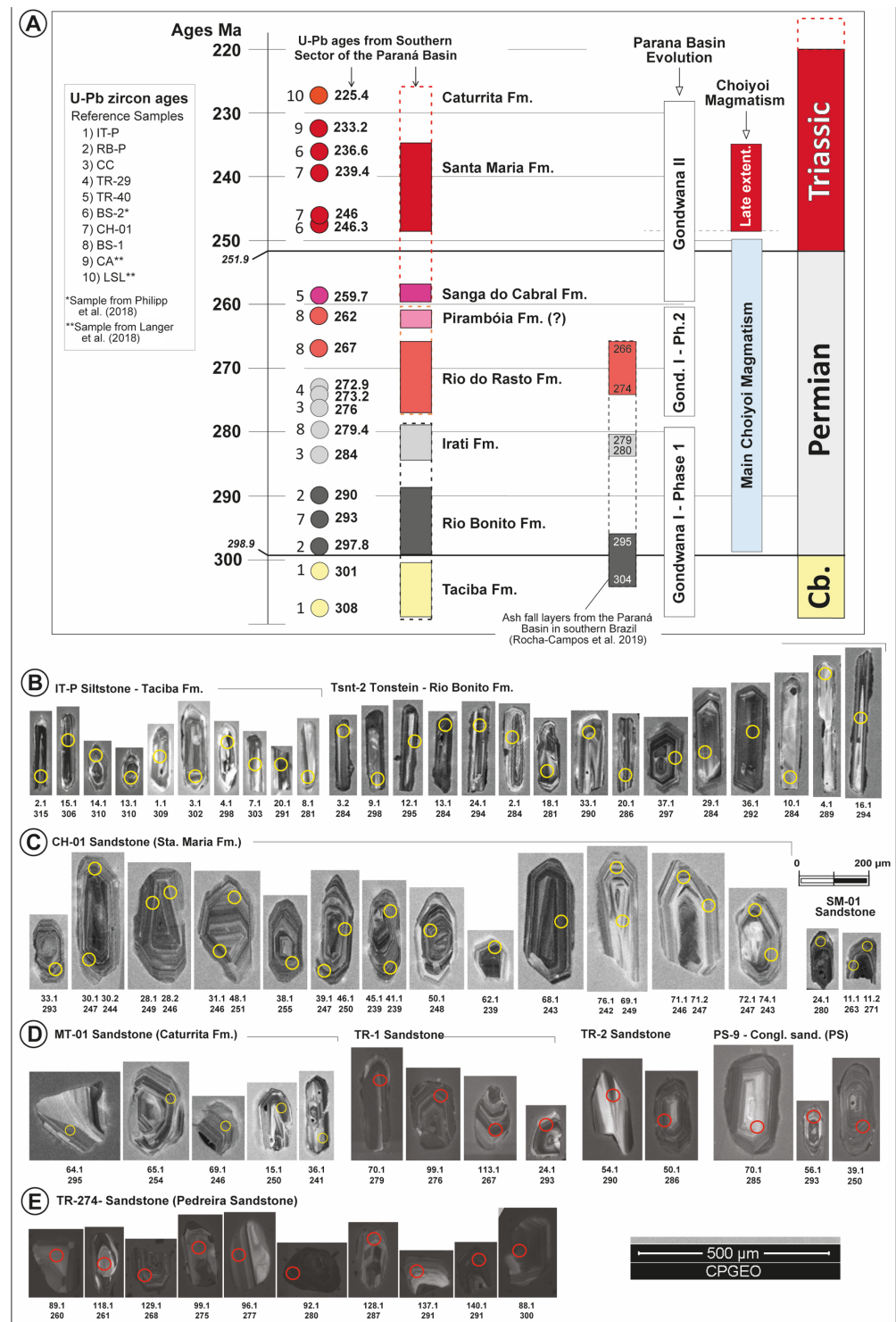


Figure 12. (A) Schematic timeline diagram showing the results of the volcanic zircon crystals from the samples of the Permian Guatá Group (Rio Bonito Formation), Passa Dois Group (Irati and Rio do Rasto Formations), and of the Rosário do Sul Group (Sanga do Cabral, Santa Maria and Caturrita Formations). (B) Cathodoluminescence (CL) images of euhedral volcanic zircons of the Itararé Group (Taciba Formation, sample IT-P), (C) Rosário do Sul Group (Santa Maria Formation, samples CH-01, SM-01), (D) Rosário do Sul Group (Caturrita Formation, sample MT-01), São Bento Group (Guará Formation and Pedreira Sandstone, samples TR-1, TR-2 and PS-9), (E) Pedreira Sandstone (sample TR-274).

The zircons aged between 260.9 and 241 Ma have a short and euhedral prismatic shape and well-developed oscillatory zonation. They do not show evidence of sedimentary reworking and are considered deposits of volcanic ashes precipitated contemporaneously with the deposition of sediments. From sample TR-40 of the lower portion of the Sanga do Cabral Formation (Rosário do Sul Group), the Concordia age of 259.7 ± 1.3 Ma (MSWD = 0.079, $n = 5$) and the $^{238}\text{U}/^{206}\text{Pb}$ weighted average age of 258.8 ± 3.7 Ma (MSWD = 0.47, $n = 3$) indicate an Upper Permian age for this deposit. The younger euhedral zircon crystals of the CH-01 from the Caturrita Formation at the top of the Rosário do Sul Group yielded a Concordia age of 239.4 ± 3.6 Ma (MSWD = 0.034, $n = 2$). An $^{238}\text{U}/^{206}\text{Pb}$ weighted average age of 245 ± 1.5 Ma (MSWD = 0.39, $n = 9$) was interpreted as being representative of reworked zircons inherited from the underlying Santa Maria Formation.

The petrographic analysis of zircon crystals along with the integration of lithostratigraphic and tectonic information allowed for the assessment of the limits of isotopic data in relation to the reworking of sedimentary rocks as “source” materials in subsequent cycles. The strata of the Passa Dois Group (Upper Permian), Rosário do Sul Group (Lower to Upper Triassic), and São Bento Group (Upper Jurassic) provide a record of the recycling of Permian sedimentary rocks (Figure 12). Volcanic crystals of the Permian age (298–271 Ma), found in the Rio Bonito and Irati formations, have been identified in the sediments of the Rosário do Sul and São Bento groups. The rounding and weathering of the grain surfaces indicate a reworking process within a new sedimentary cycle. This evidence, along with thermochronological data, supports the determination of uplift in the basement and basin, as well as the activity of the main regional NE–SW and NW–SE fault systems [35,47].

5.3. Basin Evolution

Based on the U-Pb detrital zircon results, integrated with the lithostratigraphy, facies association, sediment transport directions, and apatite fission track (AFT) data, it was possible to characterize the distinct evolutionary phases of the basin in the SW Gondwana, closely related to the Paleozoic–Mesozoic tectonic regime (Figure 1C). The lithosphere along the southern margin of Gondwana experienced regional flexure under the stresses generated along the Gondwanides belt, resulting in the creation of ‘intracratonic’ depositional space within the Gondwana shield. The growth of the continental lithosphere was a significant process during the Phanerozoic, progressively limiting marine incursions into the interior of continent [2]. Consequently, over time, the Paraná Basin, which initially opened as a gulf to the Panthalassa, became an intracratonic depression trapped within Gondwana.

The filling of the basin indicates three distinct evolutionary stages documented in the Itararé, Guatá/Passa Dois, and Rosário do Sul groups. The transitions between the Carboniferous–Permian and Permian–Triassic periods provide important evidence related to the intense continental arc magmatism, the development of fold and thrust belts (such as the Sierra de La Ventana in Argentina and the Cape Fold Belt in Africa), and intra-plate tectonic activities (Figures 14 and 15). The deposition of the earliest sedimentary strata, represented by the Itararé Group, was associated with the final stage of the Late Paleozoic Ice Age (LPIA), marking the beginning of a significant climate change and a transition from a period of glaciation [27,110] (Figure 13B). Paleocurrents analysis of this unit in the study area indicate sediment transport to the north and northwest, supporting the provenance of Paleo-Neoproterozoic zircons from the Brasiliano–Pan-African cycle rocks located to the south and southeast. The second stage was associated with a gradual climate change related to deglaciation and variations in relative sea level during the Early Permian deposition of the Guatá Group. The advancement of the sea over the continent led to the formation of flooded areas (e.g., mangroves, swamps, and estuaries), resulting in the accumulation of organic matter and extensive layers of mineral coal. This sequence, characterized by an extensive network of river systems, transitioned to estuarine and deltaic environments with predominant sediment transport to the north and northeast, as recorded in the Passa Dois Group. The uplift of the Gondwanides Belt marked the closure of the gulf and restricted ocean access, leading to the deposition of a marine succession

associated with the formation of an epicontinental sea (Guatá Sea) [109] (Figure 13). During the Upper Carboniferous and the Permian, Proterozoic and Phanerozoic orogenic belts were exposed due to regional tectonic processes (Figures 4 and 14), resulting in the deformation of sediments along the old continental margin and uplifting of the basement. This caused the formation of several foreland and associated collisional basins located to the north and northeast of the Gondwanides Belt [111,112] (Figures 1C, 14 and 15). The third stage, occurring during the Triassic, is characterized by successive tectonic pulses associated with the continuation of subduction processes and the subsequent extensional collapse of the Gondwanides Orogeny [2,4,36,37,113]. The orogenic extensional collapse promoted the uplift of the basement, located west of the current limits of the basin, and the generation of an elongated intraplate graben system (Figure 15).

The sedimentary and volcanic succession also recorded global variations in environmental conditions, including the extensive LPIA (Large Paleozoic Ice Age) [27,110,114,115], and one of the most significant episodes of climate change during the Carboniferous–Permian and Permian–Triassic, culminating in a major mass extinction event in the late Triassic and early Jurassic. These events are commonly attributed to a period of intense volcanic emissions that altered atmospheric carbon dioxide (CO₂) levels and catalyzed climate change. The abundance of Permian and Triassic prismatic and euhedral zircons corroborated to the continued volcanic activity on the SW Gondwana margin and supported previously defined lithostratigraphic data based on tetrapod vertebrate fossils, accompanied by faunal and palynological analyses. Two main pulses of intense volcanic activity and ash fall deposits were recognized in the late Permian (290–270 Ma) and Triassic (250–228 Ma), confirming that the environmental conditions and the greenhouse effect observed during the Permian were associated with the prolonged development of Choiyoi magmatism. The first episode overlaps with the regional development of Choiyoi magmatism and Carboniferous sedimentary successions, which include paralic and continental deposits with interbedded peat and coal beds. The second coincides with a rise in temperature and a massive extinction event affecting vertebrates and Triassic fauna.

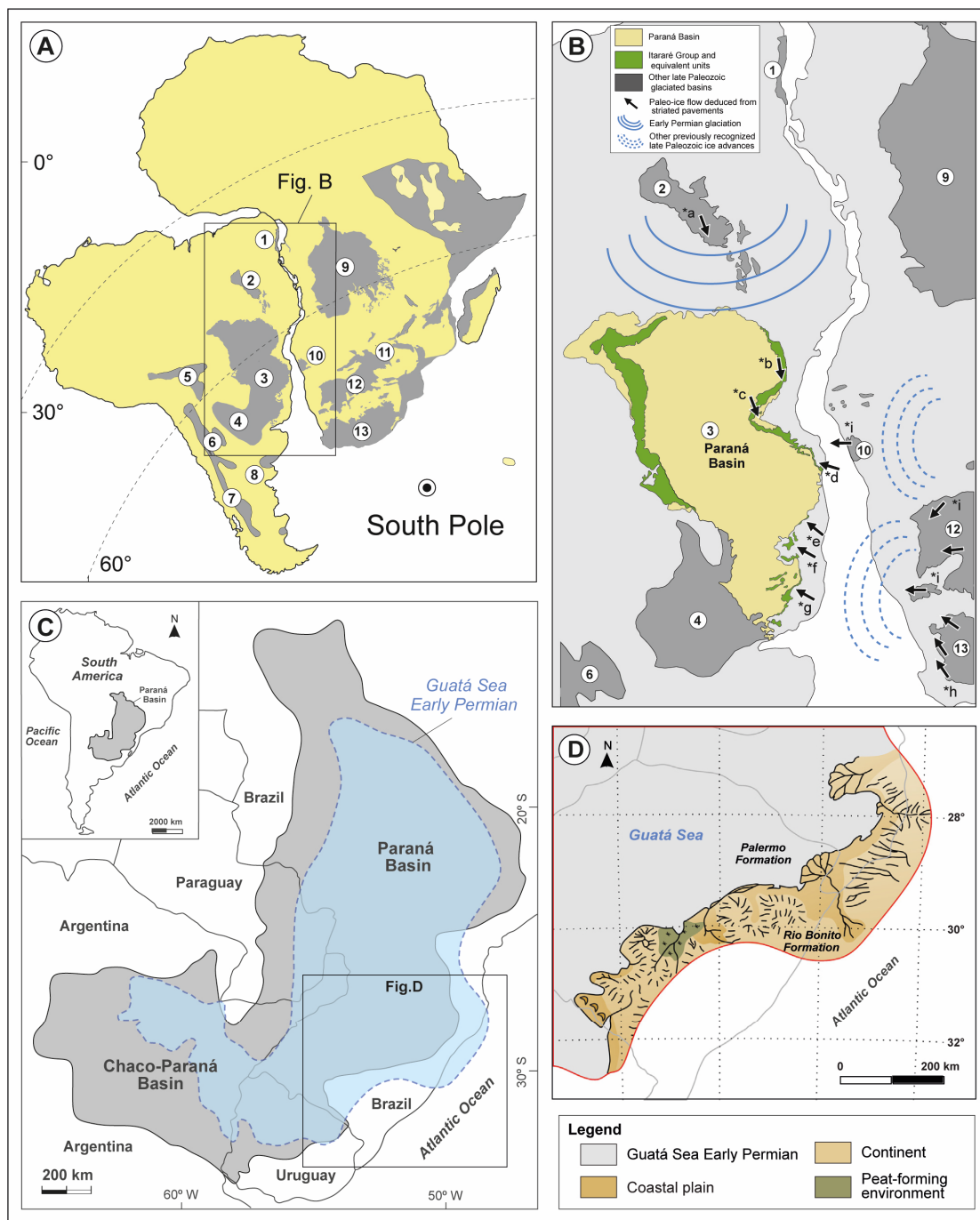


Figure 13. (A) Paleogeographic configuration of southwestern Gondwana basin system. Basins: 1—Sergipe-Alagoas, 2—Sanfranciscana, 3—Paraná, 4—Chaco-Paraná, 5—Madre de Dios, 6—Calingasta-Paganzo, 7—San Rafael, 8—Saurce Grande, 9—Congo, 10—Huab, 11—Mid-Zambeze, 12—Karoo, and 13—Kalahari. (B) Paleogeographic configuration of southwestern Gondwana during the Late Paleozoic with the distribution of the major depositional basins and the proposed paleo-ice lobe. (C) Location of the Paraná Basin and its Chaco-Paraná extension. The dashed blue line indicates the general physiography of the Guatá Sea. (D) Paleogeographic map of the southern sector of the Paraná Basin in the Early Permian. Guatá Sea corresponds to the Palermo Formation, while the coastal plain area corresponds to the Rio Bonito Fm. (brown color). The letters a* through i* indicate the sources of information for sediment transport directions. More information can be found in the References [16,46,91–93,107]. Extracted and modified from [116].

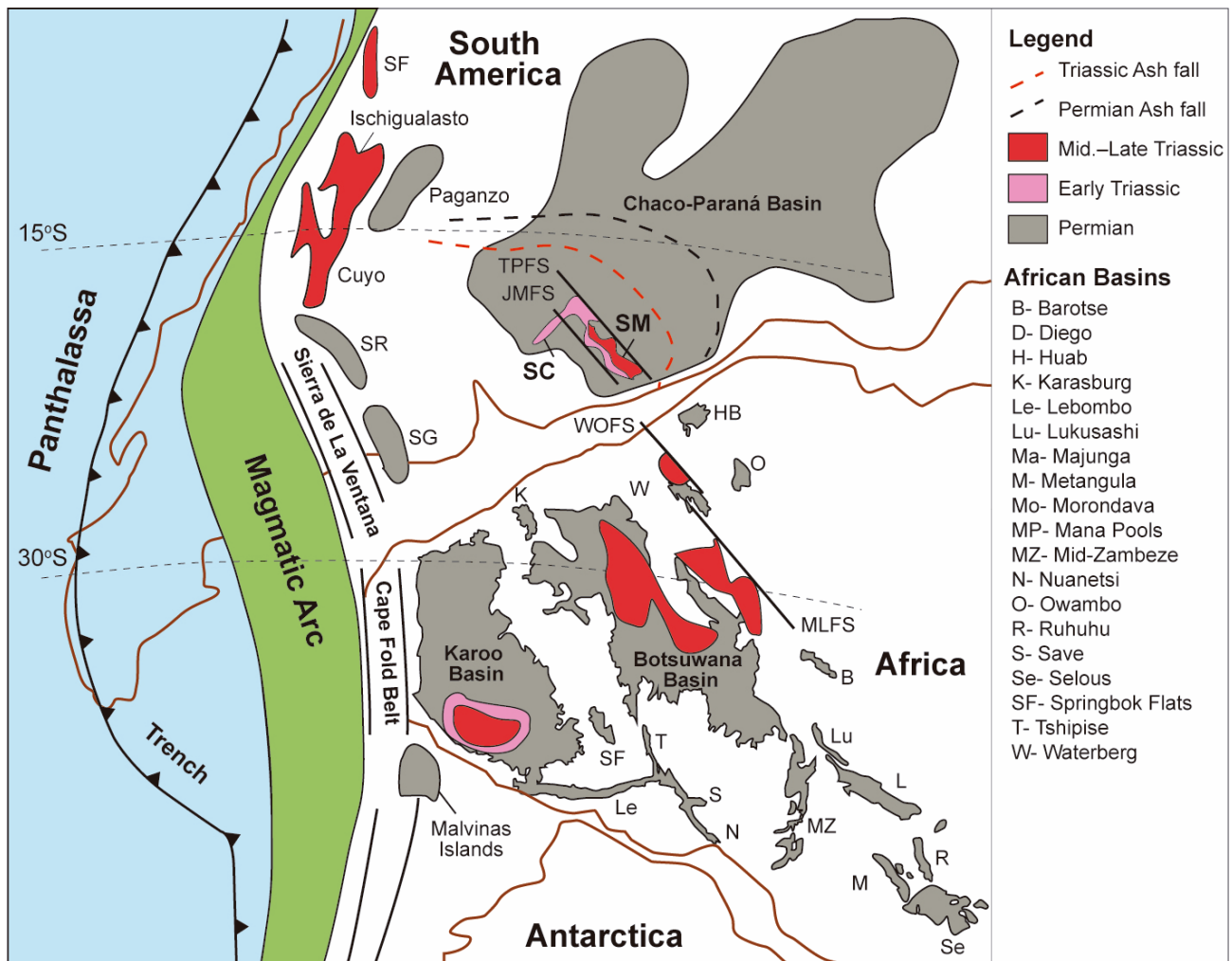


Figure 14. Paleogeographic map of southwest portion of the Gondwana showing the Permian to Triassic basins and structural features. Modified from [37] based on [7].

The origin of the structures that control the deposition sites in the study area is related to a combination of structural basement inheritance and compressive stresses generated during the development of the Gondwanides Belt [2,35,36] (Figures 1C, 14 and 15). These faults have been active since the Permian and have influenced sedimentation patterns throughout the Triassic until the Lower Cretaceous [117–119]. The N40°W-trending structures account for the formation of the Rio Grande Arch and the Torres Syncline in southern Brazil [46]. The flexural deformation of these structures is attributed to the extensional movement of large fault systems such as the Alegrete, Ibaré, Jaguari–Mata, Imbicuí, and Torres–Posadas faults, among others (Figure 4). The NE-trending faults also show evidence of reactivation records throughout the Triassic until the end of the Cretaceous, as indicated by apatite fission track (AFT) data [103,104,120].

The AFT studies conducted in the southern portion of the Atlantic and Uruguayan shields present apparent ages ranging between 383 ± 41 and 70 ± 5 Ma, defining four regional-scale tectonic events [103,104,120]. Older ages are associated with NW–SE-trending faults, whereas younger ages are related to NE–SW-trending structures. Devonian–Carboniferous ages (380–340 Ma) are exclusive to the Paleoproterozoic Taquarembó Terrane, associated with NW–SE- and NE–SW-trending fault systems. The Permian ages were recognized in samples collected in the SGT, associated with the NW–SE-trending Jaguari–Mata fault system, where two clusters were identified, one ranging from 293 to 275 Ma and another from 250 to 245 Ma. The former ages mark the unconformity within Gondwana I

sequences associated with the climax of the Gondwanides Orogeny during the Sanrafaelic Phase, whereas the later records the Gondwanides orogenic event during the extensional collapse and basement uplift. The presence of Triassic sedimentary rocks in the central portion of the Tijucas Terrane (Figure 4) suggests that this area was affected by late tectonic processes. The movement of the NW–SE trend of regional fault systems, such as Jaguari–Mata, Ibaré, and Alegrete, promoted the uplift of the basement and the erosion of the Triassic sedimentary rocks that cover the shield area. The apparent AFT ages for the easternmost Pelotas Batholith are 277–200 Ma for the NE sector, and younger ages of 190 to 150 Ma, mostly representing the initial stages of the Andean Orogeny and the early pre-drifting adjustment of the South America and Africa plates.

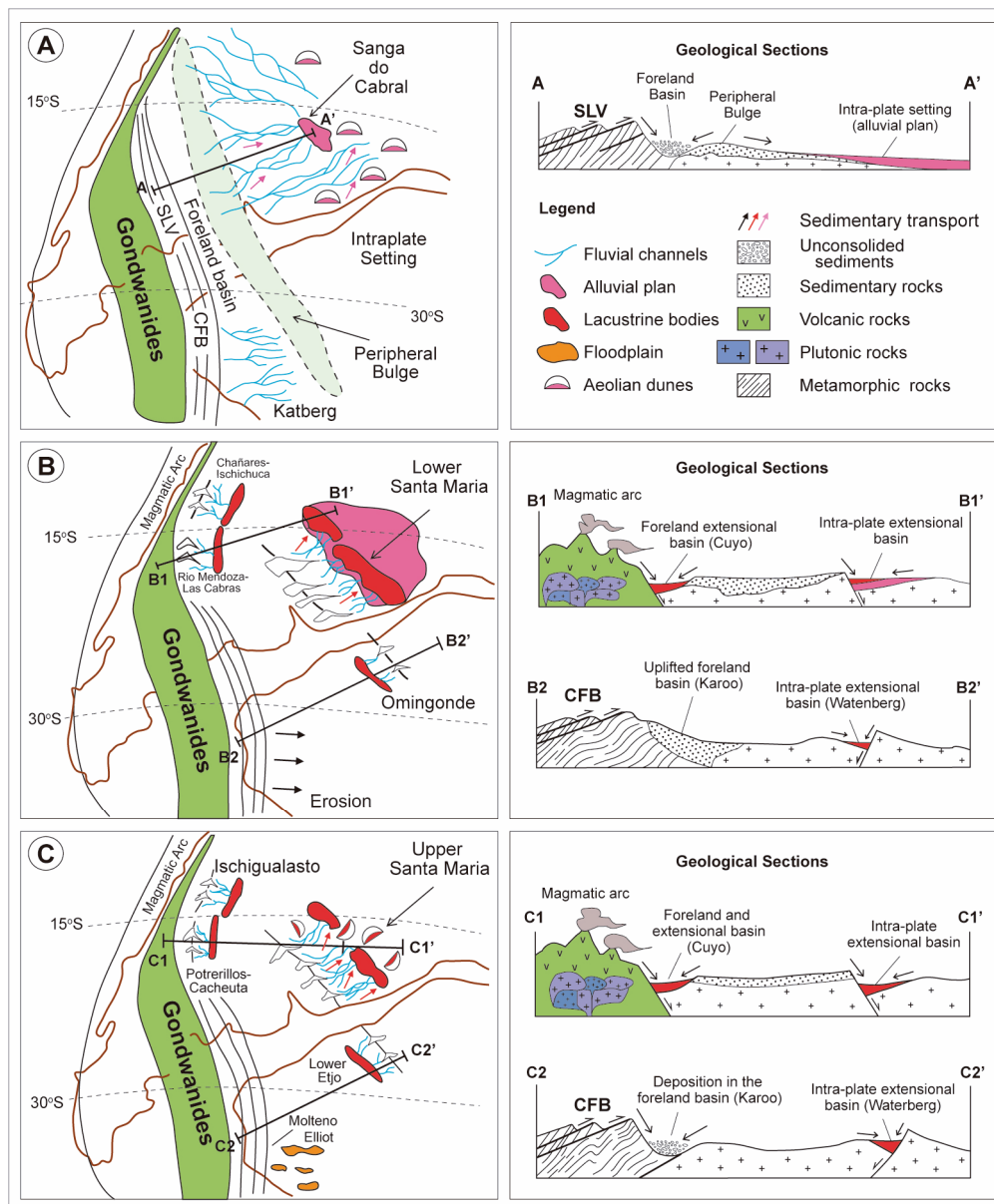


Figure 15. Paleogeographic maps and geological cross-sections of southwest Gondwana relative to the Triassic (continental margins and paleolatitudes based on [7]). (A) Early Triassic (~247 Ma) (Gondwanides I uplift); (B) Middle Triassic (~230 Ma) (Gondwanides II uplift), first stage of rifting in foreland and intraplate settings; (C) Late Triassic (~223 Ma) (Gondwanides II uplift), second stage of rifting in foreland and intraplate settings. CFB—Cape Fold Belt (South Africa), and SLV—Sierra de La Ventana (Argentina). Modified from [37].

6. Conclusions

This paper contributes to the understanding of the tectonic evolution of the southern sector of the Paraná Basin (Brazil) based on isotopic investigations of U-Pb geochronology of detrital and volcanogenic zircons from the Carboniferous to Lower Cretaceous succession. The integration of the petrographic and isotopic analysis, and sedimentological data provides useful information for provenance analysis and paleogeographic reconstruction of the entire succession in the southern sector of the basin. The paleogeographic reconstruction indicates an evolution in three distinct stages: (1) a gulf open to the Panthalassa Ocean during the Carboniferous, (2) an epicontinental sea with the rise of the Gondwanides Orogeny in the Permian, and (3) an intra-plate extensional graben system during the Triassic.

The assessment of detrital zircon provenance identifies potential source units and establishes relationships with tectonic processes during basin evolution. The data indicate sedimentary supply from the erosion of proximal and distal sources located to the south, southeast, and southwest of the basin limits. Four main age populations and their respective source areas are defined: (i) Archean to Paleoproterozoic ages from the Rio de la Plata Craton and Taquarém Terrane to the south; (ii) Mesoproterozoic grains potentially sourced from the Grenvillian basement of the Gondwanides belt in Argentina to the southwest, and Namaqua–Natal belt in Africa; (iii) Neoproterozoic ages from the Brasiliano–Pan-African Orogeny, with a major contribution from the Don Feliciano Belt; and (iv) Paleozoic populations from orogenic belts and associated foreland basin system in Argentina, as well as eroded units of the Paraná Basin.

Distinct episodes of ash fall layers in the Carboniferous–Permian and Triassic–Jurassic sections help to constrain and refine maximum depositional ages, confirming the intense volcanic activity associated with Choiyoi volcanism during the Gondwanides Orogeny. Volcanism played a catalytic role in climate change and mass extinction events that occurred during the Carboniferous to Permian and Triassic to Jurassic intervals. The widespread occurrence of ash fall deposits in the sedimentary rocks of the Paraná Basin indicates two main volcanic events between 300–270 Ma and 260–228 Ma. These events coincide with the deposition of wide coal layers and the transition to a semi-arid and later arid climate during the Triassic–Jurassic transition.

The reworking of Carboniferous and Permian zircons deposited during the Triassic provides strong evidence of the dynamics of tectonics controlling the development of regional arcs and synclines through intra-plate stress. This process resulted in the uplift of the Rio Grande Arch as a NW–SE to E–W regional structure characterized by the basement uplift processes and the subsequent erosion of early Paraná Basin units, controlling the sedimentation of the Rosario do Sul Group. This indicates a radical shift of the source-to-sink system, where older depositional sinks became the source for the subsequent sedimentary cycle.

This work demonstrates the value of the geochronological data from U-Pb zircon analysis as an important complementary tool for advancing the understanding of sedimentary basin evolution. It also highlights the importance of the lithostratigraphic record of the Paraná Basin as an example of the combined effects of tectonic activity, sedimentation, and associated climate changes. The results reinforce that the sedimentation and lithostratigraphic architecture of the Paraná Basin is the result of the influence of marginal convergent tectonic processes in an intra-cratonic setting, reflecting the behavior of the continental crust facing the demands imposed by the accretion processes along the SW margin of Gondwana.

Supplementary Materials: The following supporting information can be downloaded at <https://www.mdpi.com/article/10.3390/geosciences13080225/s1>.

Author Contributions: Conceptualization, R.P.P., C.L.S., U.F.F., G.Z., A.R.J., A.R.V. and M.A.S.B.; methodology, R.P.P., U.F.F., C.L.S., J.C., A.R.V., M.P.B., E.L. and M.A.S.B.; investigation, R.P.P., U.F.F., C.L.S., G.Z., M.P.B., A.R.V., J.C., A.R.J. and R.G.N.; resources, R.P.P., A.R.V. and U.F.F.; writing—original draft preparation, R.P.P., G.Z. and C.L.S.; writing—review and editing, R.P.P. and G.Z.; project administration, R.P.P.; funding acquisition, R.P.P. and C.L.S. All authors have read and agreed to the published version of the manuscript.

Funding: This research was funded by the Brazilian National Council for Scientific and Technological Development (CNPq).

Data Availability Statement: Not applicable.

Acknowledgments: The authors thank the editors of this volume (Andrew Morton, Shane Tyrel, and Gustavo Zvirtes) and the reviewers for the criticism and improvement of the discussions. Ruy P. Philipp express their gratitude for the research grant from the Brazilian National Council for Scientific and Technological Development (CNPq). We also thank the Geochronological Research Center (CPGEO) of the Geosciences Institute of the São Paulo University for its co-operation and for facilitating the U-Pb zircon analyses.

Conflicts of Interest: The authors declare no conflict of interest. The funders had no role in the design of the study; in the collection, analyses, or interpretation of data; in the writing of the manuscript; or in the decision to publish the results.

References

- Milani, E.J.; de Souza, P.A.; Melo, J.H.G. Bacia do Paraná. *Bol. Geociênc. Petrobras* **2007**, *15*, 265–287. [[CrossRef](#)]
- Milani, E.J.; Ramos, V. Orogenias Paleozóicas no domínio sul- ocidental do Gondwana e os ciclos de subsidência da Bacia do Paraná. *Rev. Bras. Geociênc.* **1998**, *28*, 527–544. [[CrossRef](#)]
- Veroslavsky, G.; Rossello, E.A.; López-Gamundí, O.; de Santa Ana, H.; Assine, M.L.; Marmisolle, J.; de J Perinotto, A. Late Paleozoic tectono-sedimentary evolution of eastern Chaco-Paraná Basin (Uruguay, Brazil, Argentina and Paraguay). *J. S. Am. Earth Sci.* **2021**, *106*, 102991. [[CrossRef](#)]
- Milani, E.J.; De Wit, M.J. Correlations between the classic Paraná and Cape–Karoo sequences of South America and southern Africa and their basin infills flanking the Gondwanides: Du Toit revisited. *Geol. Soc. Lond. Spec. Publ.* **2008**, *294*, 319–342. [[CrossRef](#)]
- Milani, E.J.; Faccini, U.F.; Scherer, C.M.S.; Araújo, L.M.; Cupertino, J.A. Sequences and stratigraphic hierarchy of the Paraná Basin (Ordovician to Cretaceous), Southern Brazil. *Bol. IG-USP (Sér. Cient.)* **1998**, *29*, 125–173. [[CrossRef](#)]
- Milani, E.J.; Zalán, P.V. An outline of the geology and petroleum systems of the Paleozoic interior basins of South America. *Epis. J. Int. Geosci.* **1999**, *22*, 199–205. [[CrossRef](#)]
- Rapela, C.W.; Fanning, C.M.; Casquet, C.; Pankhurst, R.J.; Spalletti, L.; Poiré, D.; Baldo, E.G. The Rio de la Plata craton and the adjoining Pan–African/brasiliano terranes: Their origins and incorporation into south-west Gondwana. *Gondwana Res.* **2011**, *20*, 673–690. [[CrossRef](#)]
- Moecher, D.P.; Samson, S.D. Differential zircon fertility of source terranes and natural bias in the detrital zircon record: Implications for sedimentary provenance analysis. *Earth Planet. Sci. Lett.* **2006**, *247*, 252–266. [[CrossRef](#)]
- Hawkesworth, C.; Dhuime, B.; Pietranik, A.; Cawood, P.; Kemp, T.; Storey, C. The generation and evolution of the continental crust. *J. Geol. Soc. Lond.* **2010**, *167*, 229–248. [[CrossRef](#)]
- Cawood, P.A.; Hawkesworth, C.J.; Dhuime, B. Detrital zircon record and tectonic setting. *Geology* **2012**, *40*, 875–878. [[CrossRef](#)]
- Gehrels, G. Detrital zircon U-Pb geochronology applied to tectonics. *Annu. Rev. Earth Planet. Sci.* **2014**, *42*, 127–149.
- Andersen, T.; Kristoffersen, M.; Elburg, M.A. How far can we trust provenance and crustal evolution information from detrital zircons? A South African case study. *Gondwana Res.* **2016**, *34*, 129–148. [[CrossRef](#)]
- Vermeesh, P. Maximum depositional age estimation revisited. *Geosci. Front.* **2021**, *12*, 843–850. [[CrossRef](#)]
- Condie, K.C.; Belousova, E.; Griffin, W.L.; Sircombe, K.N. Granitoid events in space and time: Constraints from igneous and detrital zircon age spectra. *Gondwana Res.* **2009**, *15*, 228–242. [[CrossRef](#)]
- Philipp, R.P.; Schultz, C.L.; Kloss, H.P.; Horn, B.L.D.; Soares, M.B.; Basei, M.A.S. Middle Triassic SW Gondwana paleogeography and sedimentary dispersal revealed by integration of stratigraphy and U-Pb zircon analysis: The Santa Cruz Sequence, Paraná Basin, Brazil. *J. S. Am. Earth Sci.* **2018**, *88*, 216–237. [[CrossRef](#)]
- Horn, B.L.D.; Schultz, C.L.; Philipp, R.P.; Goldberg, K.; Kloss, H.P. Definition of a new third-order sequence in the Santa Maria Supersequence (Triassic of the Paraná Basin, Rio Grande do Sul, Brazil) based in structural, stratigraphic and paleontologic data. *J. S. Am. Earth Sci.* **2014**, *55*, 123–132. [[CrossRef](#)]
- Canile, F.M.; Babinski, M.; Rocha-Campos, A.C. Evolution of the Carboniferous–Early Cretaceous units of Paraná Basin from provenance studies based on U-Pb, Hf and O isotopes from detrital zircons. *Gondwana Res.* **2016**, *40*, 142–169. [[CrossRef](#)]
- Sato, A.M.; González, P.D.; Llambias, E.J. Evolución del orógeno Famatiniano em la Sierra de San Luis: Magmatismo de arco, deformación y metamorfismo de bajo a alto grado. *Rev. Asoc. Geol. Argent.* **2003**, *58*, 34–47.

19. Andreis, R.R.; Bossi, G.E.; Montardo, D.K. O Grupo Rosário do Sul (Triássico) no Rio Grande do Sul. In *Anais do XXXI Congresso Brasileiro de Geologia, Camboriú, Santa Catarina*; Sociedade Brasileira de Geologia: Sao Paulo, Brazil, 1980; Volume 2, pp. 659–673.
20. López-Gamundi, O.R.; Espejo, I.S.; Conaghan, P.J.; Powell, C.M. Southern South America. In *Permian-Triassic Pangean Basins and Fold Belts along the Panthalassan Margin of Gondwanaland*; Veevers, J.J., Powell, C.M.A., Eds.; Geological Society of America Memoir: Fairfax County, VA, USA, 1994; Volume 184, pp. 281–329.
21. Pankhurst, R.J.; Rapela, C.W.; Saavedra, J.; Baldo, E.; Dahlquist, J.; Pasuca, L.; Fanning, C.M. The Famatinian magmatic arc in the central Sierras Pampeanas: An Early to Mid-Ordovician continental arc on the Gondwana margin. *Geol. Soc. Lond. Spec. Publ.* **1998**, *142*, 343–367.
22. Rapela, C.W.; Pankhurst, R.J.; Casquet, C.; Baldo, E.G.; Saavedra, J.; Galindo, C.; Fanning, C.M. The Pampean Orogeny of the southern proto-Andes: Cambrian continental collision in the Sierras de Córdoba. *Geol. Soc. Lond. Spec. Publ.* **1998**, *142*, 181–217. [[CrossRef](#)]
23. Otamendi, J.E.; Pinotti, L.P.; Basei, M.A.S.; Tibaldi, A.M. Evaluation of petrogenetic models for intermediate and silicic plutonic rocks from the Sierra de Valle Fértil-La Huerta, Argentina: Petrologic constrains on the origin of igneous rocks in the Ordovician Famatinian-Puna paleoarc. *J. S. Am. Earth Sci.* **2010**, *30*, 29–45. [[CrossRef](#)]
24. Dahlquist, J.A.; Pankhurst, R.J.; Rapela, C.W.; Galindo, C.; Alasino, P.; Fanning, C.M.; Saavedra, J.; Baldo, E.G. New SHRIMP U-Pb data from the Famatinian Complex: Constraining Early-Mid-Ordovician Famatinian magmatism in the Sierras Pampeanas, Argentina. *Geol. Acta* **2008**, *6*, 319–333.
25. Dahlquist, J.A.; Alasino, P.H.; Basei, M.A.S.; Morales Cámara, M.M.; Macchioli Grande, M.; Neto, M.C.C. Petrological, geochemical, isotopic, and geochronological constraints for the Late Devonian–Early Carboniferous magmatism in SW Gondwana (27–32°LS): An example of geodynamic switching. *Int. J. Earth Sci.* **2018**, *107*, 2575–2603. [[CrossRef](#)]
26. Llambías, E.J.; Quenardelle, S.; Montenegro, T. The Choiyoi Group from central Argentina: A subalkaline transitional to alkaline association in the craton adjacent to the active margin of the Gondwana continent. *J. S. Am. Earth Sci.* **2003**, *16*, 243–257. [[CrossRef](#)]
27. Buso, V.V.; Milana, J.P.; Di Pasquo, M.; Paim, P.S.G.; Philipp, R.P.; Aquino, C.D.; Cagliari, J.; Chemale, F., Jr.; Kneller, B. Timing of the Late Palaeozoic glaciation in western Gondwana: New ages and correlations from Paganzo and Paraná basins. *Palaeogeogr. Palaeoclimatol. Palaeoecol.* **2020**, *544*, 109624. [[CrossRef](#)]
28. Naipauer, M.; Tapia, F.; Mescua, J.; Farias, M.; Pimentel, M.M.; Ramos, V.A. Detrital and volcanic zircon U-Pb ages from southern Mendoza (Argentina): An insight on the source regions in the northern part of the Neuquén Basin. *J. S. Am. Earth Sci.* **2015**, *64*, 434–451. [[CrossRef](#)]
29. Schultz, C.L.; Scherer, C.M.S.; Barberena, M.C. Biostratigraphy of southern Brazilian middle-upper Triassic. *Rev. Bras. Geociênc.* **2000**, *30*, 491–494.
30. Schultz, C.L.; Martinelli, A.G.; Soares, M.B.; Pinheiro, F.L.; Kerber, L.; Horn, B.L.D.; Pretto, F.A.; Müller, R.T.; Melo, T.P. Triassic faunal successions of the Paraná Basin, southern Brazil. *J. S. Am. Earth Sci.* **2020**, *104*, 102846. [[CrossRef](#)]
31. Souza, P.A.; Marques-Toigo, M. An overview on the palynostratigraphy of the Upper Paleozoic strata of the Brazilian Paraná Basin. *Rev. Museo Argent. Cienc. Nat.* **2003**, *5*, 205–214. [[CrossRef](#)]
32. Souza, R.I.P.A. Floral succession in the lower Permian deposits of the Brazilian Paraná Basin: An up-to-date overview. In *Nonmarine Permian: Bulletin*; New Mexico Museum of Natural History and Science: Albuquerque, NM, USA, 2005; Volume 30, p. 144.
33. Cagliari, J.; Philipp, R.P.; Buso, V.V.; Netto, R.G.; Hillebrand, K.P.; Lopes, R.C.; Basei, M.A.; Faccini, U.F. Age constraints of the glaciation in the Paraná Basin: Evidence from new U–Pb dates. *J. Geol. Soc.* **2016**, *173*, 871–874. [[CrossRef](#)]
34. Tedesco, J.; Cagliari, J.; Chemale, F., Jr.; Girelli, T.; Lana, C. Provenance and paleogeography of the Southern Paraná Basin: Geochemistry and U-Pb zircon geochronology of the Carboniferous-Permian transition. *Sediment. Geol.* **2019**, *393*, 105539. [[CrossRef](#)]
35. Holz, M.; Kühle, J.; Philipp, R.P.; Bischoff, A.P.; Arima, N. Hierarchy of tectonic control on stratigraphy signatures: Base-level changes during the Early Permian in the Parana Basin, southernmost Brazil. *J. S. Am. Earth Sci.* **2006**, *22*, 185–204. [[CrossRef](#)]
36. Zerkass, H.; Lavina, E.L.; Schultz, C.L.; Garcia, A.J.V.; Faccini, U.F.; Chemale, F. Sequence stratigraphy of continental Triassic strata of Southernmost Brazil: A contribution to Southwestern Gondwana paleogeography and paleoclimate. *Sediment. Geol.* **2003**, *161*, 85–105. [[CrossRef](#)]
37. Zerkass, H.; Chemale, F.; Schultz, C.L.; Lavina, E. Tectonics and sedimentation in southern South America during Triassic. *Sediment. Geol.* **2004**, *166*, 265–292. [[CrossRef](#)]
38. Silva, L.C.; McNaughton, N.J.; Armstrong, R.; Hartmann, L.A.; Fletcher, I.R. The Neoproterozoic Mantiqueira Province and its African connections: A zircon-based U-Pb geochronologic subdivision of the Brasiliano/Pan-African systems of orogens. *Precambrian Res.* **2005**, *136*, 203–240. [[CrossRef](#)]
39. Oyhantçabal, P.; Siegesmund, S.; Wemmer, K.; Presnyakov, S.; Layer, P. Geochronological constraints on the evolution of the southern Dom Feliciano Belt (Uruguay). *J. Geol. Soc.* **2009**, *166*, 1075–1084. [[CrossRef](#)]
40. Wildner, W.; Ramgrab, G.; Lopes, R.; Da, C.; Iglesias, C.M.F. Geologia e recursos minerais do estado do Rio Grande do Sul: Escala 1:750.000. In *Programa Geologia do Brasil; Mapas Geológicos Estaduais*; CPRM: Porto Alegre, Brazil, 2007.
41. Sato, A.M.; Llambías, E.J.; Basei, A.S.; Castro, C.E. Three stages in the Late Paleozoic to Triassic magmatism of southwestern Gondwana, and the relationships with the volcanogenic events in coeval basins. *J. S. Am. Earth Sci.* **2015**, *63*, 48–69. [[CrossRef](#)]

42. Scherer, C.M.S. Eolian dunes of the Botucatu Formation (Cretaceous) in Southernmost Brazil: Morphology and origin. *Sediment. Geol.* **2000**, *137*, 63–84. [[CrossRef](#)]
43. Scherer, C.M.S.; Lavina, E.L. Stratigraphic evolution of a fluvial-eolian succession: The example of the Upper Jurassic-Lower Cretaceous Guar and Botucatu formations, Paran Basin, Southernmost Brazil. *Gondwana Res.* **2006**, *9*, 475–484. [[CrossRef](#)]
44. Rossetti, L.; Lima, E.F.; Waichel, B.; Hole, M.; Simes, M.S.; Scherer, C.M.S. Lithostratigraphy and volcanology of the Serra Geral Group, Paran-Etendeka Igneous Province in Southern Brazil: Towards a formal stratigraphical framework. *J. Volcanol. Geotherm. Res.* **2018**, *355*, 98–114. [[CrossRef](#)]
45. Thiede, D.S.; Vasconcelos, P.M. Paran flood basalts: Rapid extrusion confirmed by new ⁴⁰Ar-³⁹Ar results. *Geol. Soc. Am.* **2010**, *38*, 747–750. [[CrossRef](#)]
46. Henrique-Pinto, R.; Basei, M.A.S.; Santos, P.R.; Saad, A.R.; Milani, E.J.; Cingolani, C.A.; Frugis, G.L. Paleozoic Paran Basin transition from collisional retro-foreland to pericratonic syncline: Implications on the geodynamic model of Gondwana proto-Andean margin. *J. S. Am. Earth Sci.* **2021**, *111*, 103511. [[CrossRef](#)]
47. Philipp, R.P.; Schultz, C.L.; Faccini, U.F.; Xavier, P.; Bruckmann, M.P.; Viana, A.R.; Lana, C. U-Pb zircon dating of the Mesozoic ash-fall deposits and provenance of the Sanga do Cabral and Santa Maria supersequences, Paran Basin, Brazil. *Sediment. Geol.* **2023**, submitted.
48. Bruckmann, M.P.; Philipp, R.P.; Scherer, C.M.S.; Espndola, E.; Halfen, L. Anlise petrogrfica e provenincia do Arenito Pedreira, Jurssico Superior da Bacia do Paran, sul do Brasil. *Pesqui. Geocinc.* **2019**, *46*, e0658. [[CrossRef](#)]
49. Vermeesh, P. Isoplot R: A free and open toolbox for geochronology. *Geosci. Front.* **2018**, *9*, 1479–1493. [[CrossRef](#)]
50. Jackson, S.E.; Pearson, N.J.; Griffin, W.L.; Belousova, E.A. The application of laser ablation-inductively coupled plasma-mass spectrometry to in situ U/Pb zircon geochronology. *Chem. Geol.* **2004**, *211*, 47–69.
51. Horstwood, M.S.A.; Koler, J.; Gehrels, G.; Jackson, S.E.; McLean, N.M.; Paton, C.; Pearson, N.J.; Sircombe, K.; Sylvester, P.; Vermeesch, P.; et al. Community-Derived Standards for LA-ICP-MS U-(Th)-Pb Geochronology-Uncertainty Propagation, Age Interpretation and Data Reporting. *Geostand. Geoanal. Res.* **2016**, *40*, 311–332. [[CrossRef](#)]
52. Stacey, J.S.; Kramers, J.D. Approximation of terrestrial lead isotope evolution by a two-stage model. *Earth Planet. Sci. Lett.* **1975**, *26*, 207–221. [[CrossRef](#)]
53. Steiger, R.H.; Jger, E. Subcommittee on geochronology: Convention on the use of decay constants in geo- and cosmochronology. *Earth Planet. Sci. Lett.* **1977**, *36*, 359–369. [[CrossRef](#)]
54. Ludwig, K.R. Using Isoplot/Ex.4. A Geochronological Toolkit for Microsoft Excel. *Berkeley Geochronol. Center* **2003**, 1–47.
55. Gehrels, G. Detrital zircon U-Pb geochronology: Current methods and new opportunities. In *Tectonics of Sedimentary Basins: Recent Advances*; John Wiley and Sons: Scottsdale, AZ, USA, 2011; pp. 45–62.
56. Girelli, T.J.; Chemale, F.; Lavina, E.L.C.; Laux, J.H.; Bongioiolo, E.M.; Lana, C.C. Granulite accretion to Rio de la Plata Craton, based on zircon U-Pb-Hf isotopes: Tectonic implications for Columbia Supercontinent reconstruction. *Gondwana Res.* **2018**, *56*, 105–118.
57. Corfu, F.; Hanchar, J.M.; Hoskin, P.W.; Kinny, P. Atlas of zircon textures. *Rev. Miner. Geochem.* **2003**, *53*, 469–500. [[CrossRef](#)]
58. Unrug, R. The assembly of Gondwanaland: Episodes. *J. Int. Geosci.* **1996**, *19*, 11–20.
59. de Wit, M.J.; Jeffery, M.; Berg, H.; Nicolayson, L.O. Geological Map of sectors of Gondwana reconstructed to their position ~150 Ma (with explanatory notes), scale 1: 1,000,000 Lambert Equal Area Projection Centred at 20S, 40E. *Am. Assoc. Pet. Geol.* **1988**.
60. Eglinton, B.M. Evolution of the Namaqua-Natal Belt, southern Africa—A geochronological and isotope geochemical review. *J. Afr. Earth Sci.* **2006**, *46*, 93–111. [[CrossRef](#)]
61. Griffis, N.P.; Mundil, R.; Montnez, I.P.; Isbell, J.; Fedorchuk, N.; Vesely, F.; Iannuzzi, R.; Yin, Q. A new stratigraphic framework built on U-Pb single zircon TIMS ages and implications for the timing of the penultimate Icehouse (Paran Basin, Brazil). *GSA Bull.* **2017**, *130*, 848–858. [[CrossRef](#)]
62. Ramos, V.A. Patagonia: A Paleozoic continent adrift? *J. South Am. Earth Sci.* **2008**, *26*, 235–251. [[CrossRef](#)]
63. Warren, L.V.; Almeida, R.P.; Hachiro, J.; Machado, R.; Roldan, L.F.; Steiner, S.S.; Chamani, M.A.C. Evoluo Sedimentar da Formao Rio do Rasto (Permo-Trissico da Bacia do Paran) na poro centro-sul do estado de Santa Catarina, Brasil. *Rev. Bras. Geocinc.* **2008**, *38*, 213–227.
64. Teixeira, W.; Geraldies, M.C.; Matos, R.; Ruiz, A.S.; Saes, G.; Vargas-Mattos, G. A review of the tectonic evolution of the Sunsas belt, SW Amazonian Craton. *J. S. Am. Earth Sci.* **2010**, *29*, 47–60.
65. Basei, M.A.S.; Neves, B.B.B.; Siga, O.; Babinski, M.; Pimentel, M.M.; Tassinari, C.C.G.; Hollanda, M.H.B.; Nutman, A.; Cordani, U.G. Contribution of SHRIMP U Pb zircon geochronology to unravelling the evolution of Brazilian Neoproterozoic fold belts. *Precambrian Res.* **2010**, *183*, 112–144. [[CrossRef](#)]
66. Alessandretti, L.; Philipp, R.P.; Chemale, F., Jr.; Bruckmann, M.P.; Zvirtes, G.; Matte, V.; Ramos, V.A. Provenance, volcanic record, and tectonic setting of the Paleozoic Ventania Fold Belt and the Claromeco Foreland Basin: Implications on sedimentation and volcanism along the southwestern Gondwana margin. *J. S. Am. Earth Sci.* **2013**, *47*, 12–31. [[CrossRef](#)]
67. Ramos, V.A.; Chemale, F.; Naipauer, M.; Pazos, P.J. A provenance study of the Paleozoic Ventania System (Argentina): Transient complex sources from western and eastern Gondwana. *Gondwana Res.* **2013**, *26*, 719–740.
68. Storey, B.C.; Kyle, P.R. An active mantle mechanism for Gondwana breakup. *S. Afr. J. Geol.* **1997**, *100*, 283–290.
69. Alessandretti, L.; Machado, R.; Warren, L.V.; Assine, M.L.; Lana, C. From source-to-sink: The Late Permian SW Gondwana paleogeography and sedimentary dispersion unravelled by a multiproxy analysis. *J. S. Am. Earth Sci.* **2016**, *70*, 368–382. [[CrossRef](#)]

70. Basei, M.A.S.; Siga, O.; Masquelin, H.; Harara, O.M.; Reis Neto, J.M.; Preciozzi, F. The Dom Feliciano Belt (Brazil-Uruguay) and its foreland domain (Rio de la Plata Craton): Framework, tectonic evolution and correlation with similar provinces of Southwestern Africa. In *Tectonic Evolution of South America*; Cordani, U.G., Milani, E.J., Thomaz Filho, A., Campos, D.A., Eds.; 31 International Geological Congress: Rio de Janeiro, Brazil, 2000; pp. 311–334.
71. Saalman, K.; Gerdes, A.; Lahaye, Y.; Hartmann, L.A.; Remus, M.V.D.; Läufer, A. Multiple accretion at the eastern margin of the Rio de la Plata craton: The prolonged Brasiliano orogeny in southernmost Brazil. *Int. J. Earth Sci.* **2011**, *100*, 355–378. [[CrossRef](#)]
72. Philipp, R.P.; Pimentel, M.M.; Chemale, F., Jr. Tectonic evolution of the Dom Feliciano Belt in Southern Brazil: Geological relationships and U-Pb geochronology. *Braz. J. Geol.* **2016**, *46*, 83–104. [[CrossRef](#)]
73. Aceñolaza, G.F.; Miller, H.; Toselli, A.J. The Pampean and Famatinian cycles: Superposed orogenic events in West Gondwana. *Z. Angew. Geol.* **2000**, *1*, 337–344.
74. Philipp, R.P.; Pimentel, M.M.; Basei, M.A.S.; Salvi, M.; Lena, L.O.F.; Vedana, L.A.; Gubert, M.L.; Lopes, C.G.; Laux, J.H.; Camozzato, E. U-Pb detrital zircon dating applied to metavolcano-sedimentary complexes of the São Gabriel Terrane: New constraints on the evolution of the Dom Feliciano Belt. *J. South Am. Earth Sci.* **2021**, *110*, 103409. [[CrossRef](#)]
75. Hueck, M.; Oyhançabal, P.; Philipp, R.P.; Basei, M.A.S.; Siegesmund, S. The Dom Feliciano belt in southern Brazil and Uruguay. *Geol. Southwest Gondwana* **2018**, 267–302.
76. Lena, L.O.F.; Pimentel, M.M.; Philipp, R.P.; Armstrong, R.; Sato, K. The evolution of the Neoproterozoic São Gabriel Juvenile terrane, southern Brazil based on high spatial resolution U-Pb ages and 18O data from detrital zircon. *Precambrian Res.* **2014**, *247*, 126–138. [[CrossRef](#)]
77. Lenz, C.; Fernandes, L.A.D.; McNaughton, N.J.; Porcher, C.C.; Masquelin, H. Magmatic and metamorphic U-Pb SHRIMP ages in zircons for the Cerro Bori orthogneisses, Dom Feliciano belt in Uruguay. *Precambrian Res.* **2011**, *185*, 149–163. [[CrossRef](#)]
78. Koester, E.; Porcher, C.C.; Pimentel, M.M.; Fernandes, L.A.D.; Vignol-Lelarge, M.L.; Oliveira, L.D.; Ramos, R.C. Further evidence of 777 Ma subduction-related continental arc magmatism in Eastern Dom Feliciano Belt, southern Brazil: The Chácara das Pedras Orthogneiss. *J. S. Am. Earth Sci.* **2016**, *68*, 155–166. [[CrossRef](#)]
79. Philipp, R.P.; Zvirtes, G.; Brückmann, M.P.; Faccini, U.F.; Viana, A.R.; Lavina, E.L.C.; Scherer, C.M.S. Estruturas tectônicas na seção geológica Santana do Livramento-Rosário do Sul-Jaguari: Evidências do Arco de Rio Grande, Bacia do Paraná, RS. In Proceedings of the Boletim de Resumos Expandidos, Simpósio Nacional de Estudos Tectônicos, Chapada dos Guimarães, Brazil, 19–23 May 2013.
80. Philipp, R.P.; Bom, F.M.; Pimentel, M.M.; Junges, S.L.; Zvirtes, G. SHRIMP U-Pb age and high temperature conditions of the collisional metamorphism in the Várzea do Capivarita Complex: Implications for the origin of Pelotas Batholith, Dom Feliciano Belt, southern Brazil. *J. S. Am. Earth Sci.* **2016**, *66*, 196–207. [[CrossRef](#)]
81. Philipp, R.P.; Machado, R.; Chemale, F., Jr. Reavaliação e novos dados geocronológicos sobre o Batólito Pelotas: Implicações petrogenéticas e idade das zonas de cisalhamento. *Bol. Inst. Geociênc. USP* **2003**, *3*, 71–84.
82. Philipp, R.P.; Machado, R. The late Neoproterozoic granitoid magmatism of the Pelotas Batholith, Southern Brazil. *J. S. Am. Earth Sci.* **2005**, *19*, 461–478. [[CrossRef](#)]
83. Leite, J.A.D.; Hartmann, L.A.; McNaughton, N.J.; Chemale, F., Jr. SHRIMP U-Pb zircon geochronology of Neoproterozoic juvenile and crustal-reworked terranes in southernmost Brazil. *Int. Geol. Rev.* **1998**, *40*, 688–705. [[CrossRef](#)]
84. Saalman, K.; Remus, M.V.D.; Hartmann, L.A. Tectonic evolution of the Neoproterozoic juvenile São Gabriel belt, southern Brazil-constraints on Brasiliano orogenic evolution of the La Plata Cratonic margin. *J. S. Am. Earth Sci.* **2005**, *21*, 204–227.
85. Hartmann, L.A.; Philipp, R.P.; Santos, J.O.S.; McNaughton, N.J. Time frame of 753–680 Ma juvenile accretion during the São Gabriel Orogeny, southern Brazil. *Gondwana Res.* **2011**, *19*, 84–99. [[CrossRef](#)]
86. Arena, K.R.; Hartmann, L.A.; Lana, C.C. Evolution of Neoproterozoic ophiolites from the southern Brasiliano Orogen revealed by zircon U-Pb-Hf isotopes and geochemistry. *Precambrian Res.* **2016**, *285*, 299–314. [[CrossRef](#)]
87. Gubert, M.; Philipp, R.P.; Basei, M.A.S. Geochronology of the Bossoroca Complex, São Gabriel Terrane, Dom Feliciano belt, southern Brazil: Tectonic implications for a Neoproterozoic São Gabriel Arc. *J. S. Am. Earth Sci.* **2016**, *70*, 1–17.
88. Vedana, L.A.; Philipp, R.P.; Basei, M.A.S. Tonian to early Cryogenian synorogenic basin of the São Gabriel Terrane, Dom Feliciano Belt, southernmost Brazil. *Int. Geol. Rev.* **2017**, *60*, 109–133. [[CrossRef](#)]
89. Hartmann, L.A.; Santos, J.O.S.; Leite, J.A.D.; Porcher, C.C.; McNaughton, N.J. Metamorphic evolution and U-Pb zircon SHRIMP geochronology of the Belizário ultramafic amphibolite, Encantadas Complex, southernmost Brazil. *An. Acad. Bras. Ciênc.* **2003**, *75*, 393–403. [[CrossRef](#)]
90. Camozzato, E.; Lopes, R.C.; Philipp, R.P. Geologia e recursos minerais da Folha Hulha Negra, SH.22-Y-C-I, Escala 1:100.000, Estado do Rio Grande do Sul. In *Programa Geologia do Brasil*; CPRM: Porto Alegre, Brazil, 2017; p. 162.
91. Remus, M.V.D.; Hartmann, L.A.; McNaughton, N.J.; Groves, D.I.; Fletcher, I.R. The link between hydrothermal epigenetic copper mineralization and the Caçapava Granite of the Brasiliano Cycle in southern Brazil. *J. S. Am. Earth Sci.* **2000**, *13*, 191–216. [[CrossRef](#)]
92. Matté, V.; Sommer, C.A.; Lima, E.F.; Philipp, R.P.; Basei, M.A.S. Post-collisional Ediacaran volcanism in oriental Ramada plateau, southern Brazil. *J. S. Am. Earth Sci.* **2016**, *71*, 201–222. [[CrossRef](#)]
93. Oliveira, D.S.; Sommer, C.A.; Philipp, R.P.; Lima, E.F.; Basei, M.A.S. Post-collisional subvolcanic rhyolites associated to the Neoproterozoic Batholith Pelotas, Southern Brazil. *J. S. Am. Earth Sci.* **2015**, *63*, 84–100. [[CrossRef](#)]

94. Gregory, T.R.; Bitencourt, M.F.; Nardi, L.V.; Florisbal, L.M.; Chemale, F., Jr. Geochronological data from TTG-type rock associations of the Arroio dos Ratos Complex and implications for crustal evolution of southernmost Brazil in Paleoproterozoic times. *J. S. Am. Earth Sci.* **2015**, *57*, 49–60. [[CrossRef](#)]
95. Uliana, M.A.; Biddle, K.T. Mesozoic-Cenozoic paleogeographic and geodynamic evolution of southern South America. *Rev. Bras. Geociênc.* **1988**, *18*, 172–190. [[CrossRef](#)]
96. Chericoff, C.J.; Zappettini, E.O.; Santos, J.O.S.; Allchurch, S.; McNaughton, N.J. The southern segment of the Famatinian magmatic arc, La Pampa Province, Argentina. *Gondwana Res.* **2010**, *4*, 662–675. [[CrossRef](#)]
97. Rocha-Campos, A.C.; Basei, M.A.S.; Nutman, A.P.; Santos, P.R.; Passarelli, C.R.; Canile, F.M.; Rosa, O.C.R.; Fernandes, M.T.; Santa Ana, H.; Veroslavsky, G. U-Pb zircon dating of ash fall deposits from the upper Paleozoic Paraná Basin of Brazil and Uruguay: A re-evaluation of the stratigraphic correlations. *J. Geol.* **2019**, *27*, 167–182. [[CrossRef](#)]
98. López Gamundi, O. Permian plate margin volcanism and tuffs in adjacent basins of west Gondwana: Age constraints and common characteristics. *J. S. Am. Earth Sci.* **2006**, *22*, 227–238. [[CrossRef](#)]
99. Spalletti, L.; Limarino, C.O. The Choiyoi magmatism in southwestern Gondwana: Implications for the end-permian mass extinction—A review. *Andean Geol.* **2017**, *44*, 328–338. [[CrossRef](#)]
100. Rocha-Campos, A.C.; Basei, M.A.S.; Nutman, A.P.; Kleiman, L.E.; Varela, R.; Llambias, E.; Canile, F.M.; da Rosa, O. 30 million years of Permian volcanism recorded in the Choiyoi igneous province (W Argentina) and their source for younger ash fall deposits in the Parana Basin: SHRIMP U-Pb zircon geochronology evidence. *Gondwana Res.* **2011**, *19*, 509–523. [[CrossRef](#)]
101. Langer, M.C.; Ramezani, J.; Da Rosa, A.A.S. U-Pb age constraints on dinosaur rise from south Brazil. *Gondwana Res.* **2018**, *57*, 133–140. [[CrossRef](#)]
102. Guerra-Sommer, M.; Cazzulo-Klepzig, M.; Laquintinie Formoso, M.L.; Menegat, R.; Mendonça, J.G. U-Pb dating of tonstein layers from a coal succession of the southern Paraná Basin (Brazil): A new geochronological approach. *Gondwana Res.* **2008**, *14*, 474–482. [[CrossRef](#)]
103. Oliveira, C.H.E.; Jelinek, A.R.; Chemale Jr., F.; Bernet, M. Evidence of post-Gondwana breakup in Southern Brazilian Shield: Insights from apatite and zircon fission track thermochronology. *Tectonophysics* **2016**, *666*, 173–187. [[CrossRef](#)]
104. Jelinek, A.R.; Philipp, R.P.; Chemale, F., Jr.; Faccini, U.F.; Viana, A.R.; Lavina, E.L.C. The tectonic-thermal history of the Southern Brazilian Shield and the relation to the depositional history of Paraná Basin. In Proceedings of the International Congress of Thermochronology Abstract Book, Chamonix, France, 8–12 September 2014; Volume 11, p. 1.
105. Machado, J.P.S.L.; Jelinek, A.R.; Bicca, M.M.; Stephenson, R.; Genezini, F.A. West Gondwana orogenies and Pangaea break-up: Thermotectonic effects on the southernmost Mantiqueira Province, Brazil. *J. Geol. Soc.* **2019**, *176*, 1056–1075. [[CrossRef](#)]
106. Storey, B.C.; Leat, P.T.; Ferris, J.K. The location of mantle-plume centers during the initial stages of Gondwana break-up. In *Mantle Plumes: Their Identification through Time*; Ernst, R.E., Buchan, K.L., Eds.; Geological Society of America Special Papers: Fairfax County, VA, USA, 2001; Volume 352, pp. 71–80.
107. Hervé, F.; Haller, M.J.; Duhart, P.; Fanning, C.M. SHRIMP U-Pb ages of detrital zircons from Cushamen and Esquel formations, North Patagonian Massif, Argentina: Geological implications. In *Congreso Geológico Argentino*; Actas La Plata, 2005; pp. 309–314.
108. Navarrete, C.; Gianni, G.; Encinas, A.; Márquez, M.; Kamerbeek, Y.; Valle, M.; Folguera, A. Triassic to Middle Jurassic geodynamic evolution of southwestern Gondwana: From a large flat-slab to mantle plume suction in a rollback subduction setting. *Earth-Sci. Rev.* **2019**, *194*, 125–159. [[CrossRef](#)]
109. Candido, M.; Cagliari, J.; Lavina, E.L. Tidal circulation in an Early Permian epicontinental sea: Evidence of an amphidromic system. *Palaeogeogr. Palaeoclimatol. Palaeoecol.* **2020**, *546*, 109671. [[CrossRef](#)]
110. Buso, V.V.; Aquino, C.D.; Paim, P.S.G.; Souza, P.A.; Mori, A.L.; Fallgatter, C.; Milana, J.P.; Kneller, B. Late Paleozoic glacial cycles and subcycles in western Gondwana: Correlation of surface and subsurface data of the Paraná Basin, Brazil. *Palaeogeogr. Palaeoclimatol. Palaeoecol.* **2019**, *531*, 108435. [[CrossRef](#)]
111. Veevers, J.J. Gondwanaland from 650–500 Ma assembly through 320 Ma merger in Pangea to 185–100 Ma breakup: Supercontinental tectonics via stratigraphy and radiometric dating. *Earth Sci. Rev.* **2004**, *68*, 1–132. [[CrossRef](#)]
112. Limarino, C.O.; Spalletti, L.A. Paleogeography of the upper Paleozoic basins of southern South America: An overview. *J. S. Am. Earth Sci.* **2006**, *22*, 134–155. [[CrossRef](#)]
113. De Wit, M.J.; Ransome, I.G.D. Regional inversion tectonics along the southern margin of Gondwana. In *Inversion Tectonics of the Cape Fold Belt, in Karoo and Cretaceous Basins of Southern Africa*; De Wit, M.J., Ransome, I.G.D., Eds.; Balkema: Rotterdam, The Netherlands, 1992.
114. Vesely, F.F.; Assine, M.L. Deglaciation sequences in the Permo-Carboniferous Itararé Group, Paraná Basin, southern Brazil. *J. S. Am. Earth Sci.* **2006**, *22*, 156–168. [[CrossRef](#)]
115. Tedesco, J.; Cagliari, J.; Coitinho, J.D.R.; Lopes, R.C.; Lavina, E.L.C. Late Paleozoic paleofjord in the southernmost Parana Basin (Brazil): Geomorphology and sedimentary fill. *Geomorphology* **2016**, *269*, 203–214. [[CrossRef](#)]
116. Veevers, J.J.; Powell, C.; Collinson, J.W.; López-Gamundi, O.R. Synthesis. Permian-Triassic Basins and Fold belts along the Panthalassan Margin of Gondwanaland. *Geol. Soc. Am. Mem.* **1994**, *184*, 331–935.
117. Cruz, R.; Basei, M.A.S.; Philipp, R.P.; Iglesias, C.M.F. Insights into the evolution of the southeastern Dom Feliciano Belt and its connection to the Pan-African Orogeny based on new U-Pb and Lu-Hf zircon data. *Precambrian Res.* **2023**, *388*, 106955. [[CrossRef](#)]
118. Zerfass, H.; Chemale, F., Jr.; Lavina, E.L.C. Tectonic Control of the Triassic Santa Maria Supersequence of the Paraná Basin, Southernmost Brazil, and its Correlation to the Waterberg Basin, Namibia. *Gondwana Res.* **2005**, *2*, 163–176. [[CrossRef](#)]

119. Waichel, B.L.; Lima, E.F.; Viana, A.R.; Scherer, C.M.; Bueno, G.V.; Dutra, G. Stratigraphy and volcanic facies architecture of the Torres syncline, southern Brazil, and its role in understanding the Paraná-Etendeka continental flood Basalt Province. *J. Volcanol. Geotherm. Res.* **2012**, *215*, 74–82. [[CrossRef](#)]
120. Machado, J.P.S.L.; Jelinek, A.R.; Bicca, M.M.; Stephenson, R.; Randell, O.; Sullivan, P. Thermochronology of South America passive margin between Uruguay and southern Brazil: A lengthy and complex cooling history based on (U-Th)/He and fission tracks. *J. S. Am. Earth Sci.* **2021**, *106*, 103019. [[CrossRef](#)]

Disclaimer/Publisher's Note: The statements, opinions and data contained in all publications are solely those of the individual author(s) and contributor(s) and not of MDPI and/or the editor(s). MDPI and/or the editor(s) disclaim responsibility for any injury to people or property resulting from any ideas, methods, instructions or products referred to in the content.